3 Quantized transport

While the conductance quantization observed in ballistic QPCs can be naïvely understood as the perfect transmission of the one-dimensional subbands defined in the ballistic constriction this explanation raises many fundamental issues. Here an overview of the important theoretical results and predictions is presented, and the relevant experimental data provided and discussed.

3.1 Overview of the theory

The current carried in a single one-dimensional subband can readily be shown to be related to the integral over the product of the density of states, $D(\epsilon)$, and the velocity, $v(\epsilon)$, of the electrons. Regardless of the exact nature of the subband dispersion this product can be simply rewritten as

$$D(\epsilon) \cdot v(\epsilon) = D(k)\frac{\mathrm{d}k}{\mathrm{d}\epsilon} \cdot \frac{1}{\hbar}\frac{\mathrm{d}\epsilon}{\mathrm{d}k} = \frac{1}{\pi\hbar}. \tag{40}$$

In the linear response limit this cancellation gives rise to a current per subband of $(e^2/\pi\hbar)V$ where V is the voltage applied between the reservoirs. This is the conductance quantization and the observation of conductance steps of magnitude $2e^2/h$ suggests simply that the number of one-dimensional subbands has changed accordingly, and that the conductance of each subband adds as expected in a parallel configuration. While this explanation could be plausible for a long one-dimensional channel with translational invariance along its length, it is difficult to see how it applies directly to the narrow constriction of a ballistic QPC. Shortly after the experimental observation of conductance quantization a number of theoretical approaches appeared to explain the effect in more detail. Broadly speaking two distinct approaches to the problem were considered; adiabatic models in which the confining potential of the QPC gives rise to a smooth transition, and hence transmission, of the one-dimensional modes, or alternatively wavefunction matching schemes in which the perfect transmission results from a perfect coupling to the channel modes. While both approaches manifest many similarities, and indeed provide an excellent description of the quantization, several subtle differences arise which warrant particular attention.

3.1.1 The adiabatic model

The essence of the adiabatic model of transmission in a ballistic QPC is that the lateral confinement generated by the split-gate electrode configuration results in a slowly varying potential along the length of the QPC (Fig. 13).

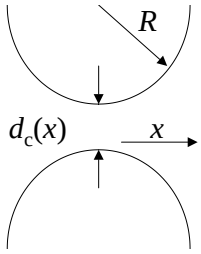

Fig. 13: The geometry assumed within the simple adiabatic model [88G2] is schematically illustrated. Only within the central region, $x \ll R$, is the adiabatic approximation strictly valid.

The variation in width of this confining potential is required to be small at the scale of the Fermi wavelength. Under such conditions an adiabatic separation of variables in the Schrödinger equation is possible [88G2],

$$-\frac{\hbar^2}{2m^*}\frac{\mathrm{d}^2\psi}{\mathrm{d}x^2} + \epsilon_n(x)\psi = E\psi \tag{41}$$

with the quantization energies

$$\epsilon_n(x) = \frac{\pi^2 n^2 \hbar^2}{2m^* d^2(x)} \tag{42}$$

where $d(x)$ is the position dependent width of the narrow constriction, and n the 1D subband index. The quantization in the 2D plane is here ignored and the confining potential is assumed to be hard walled. The corresponding solutions of the one-dimensional Schrödinger equation are either travelling waves or exponentially damped solutions, depending upon the value of $E - \epsilon_n(x)$. The narrowest point of the constriction $d_c = d(x_c)$ thus determines the critical energies $\epsilon_n(x_c)$ and hence the number of one-dimensional channels contributing to the conductance.

Within the adiabatic model the wavefunctions associated with each subband are smoothly transformed along the channel and there is no wavefunction mixing between subbands. Hence the naïve calculation of conductance discussed above remains valid, and the total conductance is given simply by $(2e^2/h)n_c$ where $n_c = \mathrm{Int}[k_F d_c/\pi]$, i.e. the number of subbands with critical energy smaller than the Fermi energy. The smooth variation assumed above for the channel geometry leads to a particularly simple formula for the transition region between quantized steps in conductance,

$$\delta G = \frac{2e^2}{h} \frac{1}{1 + \exp(-z\pi^2\sqrt{2R/d_c})} \tag{43}$$

where R is the radius of curvature of the constriction at its narrowest point and $z = (k_F d_c/\pi - n_c)$ a parameter to describe the continuous change in k_F (or energy) required for the observation of a conductance step. It is important to note that the adiabaticity assumed in this model is strictly local; the gradual variation of the width will inevitably break down at the interface between QPC and reservoirs. However, providing the length of the constriction is significantly larger than $\sqrt{Rd_c}$ then these accommodation regions do not contribute to the QPC resistance.

3.1.2 The Wide-Narrow-Wide geometry

An alternative description of the conductance quantization can be given by considering the transmission in the so-called Wide-Narrow-Wide (WNW) geometry [89S6]. In this geometry the width of the conducting region changes abruptly at the entrance to the QPC and remains constant along the channel length, as shown in Fig. 14.

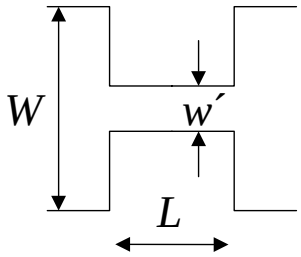

Fig. 14: The wide-narrow-wide geometry considered in the text is schematically illustrated. Both the length L and the width w' are comparable with the Fermi wavelength, and W is considered macroscopic.

In order to calculate the conductance the scattering matrix for the system must be determined. Although there is still some debate as to which version of the Landauer-Büttiker formula is most appropriate for such a calculation the correct result can be derived from the two-terminal formula

$$G = \frac{2e^2}{h} \sum_{nm} |t_{nm}|^2. \tag{44}$$

Here t_{nm} are the transmission amplitudes between tranverse modes m and n far from the constriction. The essence of the problem lies in the mode conversion which takes place at the entrance and exit of the QPC. Even in the absence of adiabatic transport, as discussed above, the states with lateral-quantization energy well below the Fermi energy couple well to the reservoirs and are almost perfectly transmitted ($T_n = |t_{nn}|^2 \approx 1$). Indeed, for the simplified problem of a semi-infinite channel the transmission approaches unity very quickly as a function of the dimensionless parameter $\Delta = k_F w'/\pi$ as shown in Fig. 15.

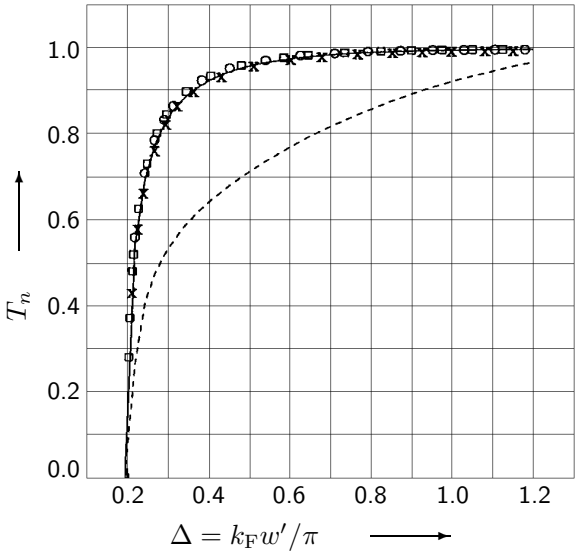

Fig. 15: The transmission coefficient T_n for a Wide-Narrow-geometry is plotted as a function of the dimensionless parameter $\Delta = k_F w'/\pi$ for various numerical models and theoretical approximations [89S6].

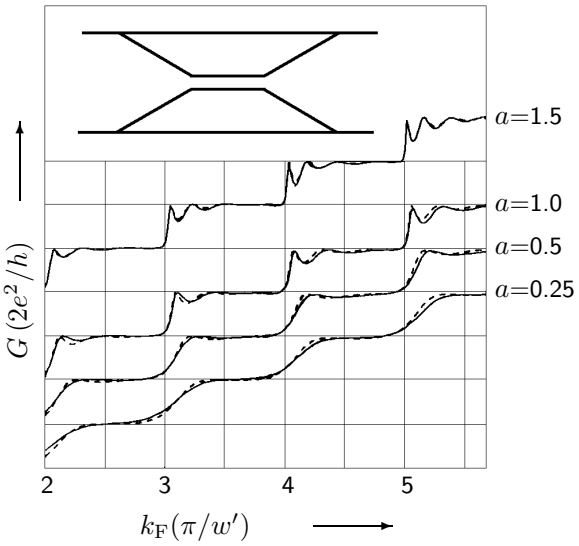

Fig. 16: The conductance $G(\epsilon_F)$ for various aspect ratios $a = L/w'$. The dashed line of the top trace is the weakly modified conductance due to tapering [89S6]. Inset is the tapering geometry assumed for $a = 1.5$.

A further important result of the WNW model lies in the dependence of the calculated transmission upon the channel aspect ratio L/w'. The coherent reflection of the channel modes leads to resonant structure in the transmission for large aspect ratios. The resonant structure is most pronounced at the onset of transmission and decays rapidly as the transmission coefficient approaches unity for large energies. Nevertheless, the calculated resonant structure is comparatively robust and is not significantly damped when a tapering between the QPC channel and the wide reservoirs is included, as illustrated in Fig. 16 for an aspect ratio of $a = 0.25$.

3.1.3 Quantization

An elegant analytical solution for an adiabatic channel is that for hard-walled hyperbolic confinement [89K1], where

$$\frac{y^2}{(c\cos\alpha)^2} - \frac{x^2}{(c\sin\alpha)^2} = 1 \tag{45}$$

defines the explicit form of the hyperbola. In such a system the separation of the variables can be achieved using (modified) Mathieu functions and elliptic coordinates. The current through the QPC is then evaluated using linear response and a knowledge of the current-density operator within the 2D-plane. The calculated conductance quantization shows well-defined steps which qualitatively improve for larger values of the asymptotic angle α (see Fig. 17).

A related adiabatic model which removes the necessity for hard-walled confinement has also been considered [90B2]; here the confining potential in the 2D-plane is taken to be

$$V(x,y) = V_0 - \frac{1}{2}m{\omega_x}^2x^2 + \frac{1}{2}m{\omega_y}^2y^2. \tag{46}$$

The separation of the motion in such a saddle point constriction is straightforward and the resulting transmission easy to calculate. Steps in the conductance are derived as a function of the Fermi energy of the system, where the energy interval required for each step is determined by $\hbar\omega_y$ as shown in Fig. 18. Clear quantization is expected when $\hbar\omega_y \geq \hbar\omega_x$.

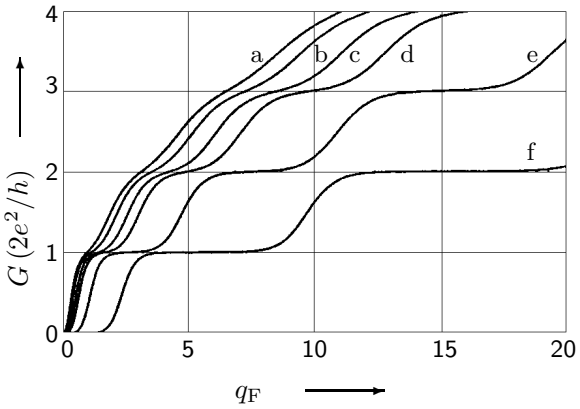

Fig. 17: The conductance of the hyperbolic constriction as a function of the normalised energy parameter $q_F = m\epsilon_F c^2/2\hbar^2$. The various traces (a,...,f) correspond to values of the asymptotic $\alpha = 0$, $\pi/16$, $\pi/8$, $\pi/6$, $\pi/4$, and $\pi/3$, respectively [89K1].

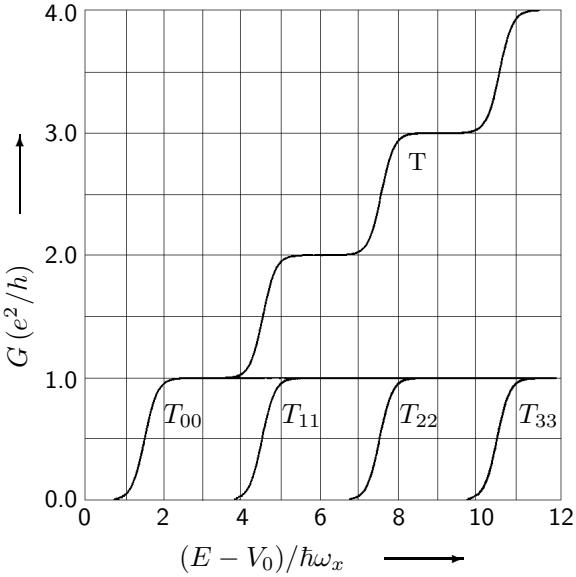

Fig. 18: The single-channel T_{nn} and total transmission probabilities as a function of energy in units of $\hbar\omega_x$ [90B2] for $\hbar\omega_y = 3\hbar\omega_x$. As explained in the text clear quantization in units of $(n + 1/2)\hbar\omega_y$ is observed in the limit of $\hbar\omega_y \gg \hbar\omega_x$. The quantized conductance in units of e^2/h results from an omission of the spin degeneracy.

Many of the early theoretical publications which attempted to explain the conductance quantization relied upon simple WNW geometries with either hard-walled or parabolic confinement in the direction perpendicular to the current. An interesting feature which was found in a number of papers [88I, 93X] was the expectation that the conductance quantization is not specific to 2D-structures and could in theory also be observed for systems with many occupied 2D-states, i.e. in systems of finite lateral extent in both directions perpendicular to the transport direction. Indeed for the 3D-1D-3D structure [93X] with square cross-section conductance steps of magntiude $4e^2/h$ result from the possible mode degeneracy within the constriction itself. The treatment of the QPC boundaries to the surrounding reservoirs is critical, and even in WNW structures artificial adiabaticity has been invoked [88I] to reproduce qualitatively the experimental quantization. In a WNW geometry with parabolic confinement [88K2, 89K5] the effect of resonant coupling between the reservoirs has been investigated as a function of channel length (see Fig. 19). The resonant peaks in the conductance are associated with length resonances where the channel length is equal to an integral number of half wavelengths of the Fermi electrons. Interestingly these modes have to be adjusted for weak end effects and can be understood as the electronic analogue of the acoustic modes of an open organ pipe.

An interesting extension of the picture of resonant transmission considers the diffraction of the electronic waves at the entrance and exit to the QPC [88L2]. In a particularly elegant derivation, which exploits the reciprocity principle, the channel conductance for a single subband can be shown to be given by

$$G = \frac{e^2}{\pi\hbar}\frac{|T|^4}{4(1-|T|^2)\sin^2\phi + |T|^4} \tag{47}$$

where ϕ is the phase shift along the length of the constriction, and $|T|$ the transmission at the entrance integrated over all angles for fixed energy. A quantized conductance is attained either when there is no diffraction at the exit of the constriction, or when there is resonant transmission

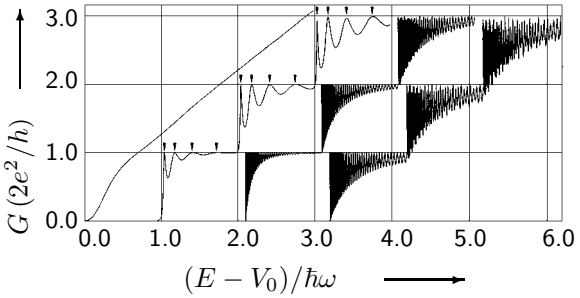

Fig. 19: The conductance for various aspect ratios L/w' (a: 0.5, b: 5, c,d: 50) as a function of normalized energy [88K2]. The curves b,c and d are offset horizontally for clarity.

($\sin\phi = 0$). The latter effect is most important as the modes are switched into the conductance, while the former is the case for the high-energy limit and explains the quantization seen in this limit.

WNW geometries have also been considered within the framework of tight-binding Hamiltonians [89H2, 89vdM, 89H3, 93H1]. The ballistic constriction itself can be modelled as a simple aperture within the 2D-lattice, or indeed as a set of lattice points with arbitrary geometry [89H2, 89vdM]. Using this technique it has been found that the conductance quantization is most clearly visible for channel lengths $L_c \approx 0.32\sqrt{n}\lambda_F$ where n is the subband index; for shorter channels the increase in conductance with width (or equally Fermi energy) is almost monotonic, while for longer channels the resonant structure becomes pronounced and leads to significant deviations from quantization. Alternatively, the QPC can be modelled with additional tight-binding reservoirs [89H3, 93H1] with considerably more lattice points. Systematic studies which include the influence of scattering have been performed using this technique and are discussed below. A tight-binding Hamiltonian defined on a rectangular lattice has also been investigated in a simpler geometry [88K4, 89M]; here the reservoirs were incorporated into the rectangular lattice, albeit as field free regions. The translational invariance defined in this geometry implicitly yields a truly one-dimensional channel; the expected conductance quantization was derived and, in contrast with the WNW models, found to be independent of channel length.

A cylindrical geometry [88J], whose circumference models the channel length, has been invoked in analogy with similar models of the quantum Hall effect (QHE). In this geometry the definition of an applied voltage can only be indirectly derived through differing chemical potentials for the two directions of motion around the cylinder. The authors are nevertheless able to determine the device conductance and suggest that the zero-temperature two-terminal conductance in the absence of all scattering is always quantized, regardless of the actual constriction width.

Clearly, the quantized conductance can be explicitly derived within the framework of a large number of alternative theoretical descriptions. Both within the adiabatic model and WNW models it is explained as the perfect transmission of the finite number of occupied modes in the constriction. The somewhat suprising fact that a 'perfect' conductor can have a finite resistance has now been understood as the inevitable contact resistance between constriction and reservoirs. In the context of the Landauer-Büttiker formalism (see Eqn. (44) above) the perfect transmission of channel modes $t_{nm} \approx \delta_{nm}$ means that mixing between the transverse modes is unimportant. While this picture gives us a good description of such non-local properties as the two-terminal conductance, a microscopic picture of the local electrostatic potential, and local density of states is lacking. The former problem has been addressed using an exact formulation of the Landauer resistivity dipole [91Z, 98U] for a simple model potential. It has been shown that the voltage drop along the channel is approximately linear, is concentrated symmetrically at the entrance and exit to the QPC, and that there is no potential drop at the narrowest point of the QPC, in marked contrast to a classical, diffusive channel.

Finally, a somewhat exotic derivation of the quantized conductance has been given from a thermodynamic analysis of the quantum electrodynamical properties of a one-dimensional system [88W3]. The quantized result is explained as the radiative impedance of a one-dimensional transmission line, whose impedance can be related to the capacitance and inductance per length.

3.1.4 Finite temperature

The effect of a finite temperature on the conductance of a QPC will be determined by the temperature dependence of the Fermi distribution and the consequent occupation of electronic states at the Fermi energy. In adiabatic models this leads to a thermal broadening of the conductance steps between quantized values for [88G2]

$$k_{\mathrm{B}}T > \frac{n\hbar^2}{m\sqrt{2Rd_{\mathrm{c}}^3}} \tag{48}$$

when thermal broadening exceeds the broadening related to the geometry as given in Eqn. (43) above. For WNW models the effects of finite temperature are twofold: first at intermediate temperatures the oscillatory structure resulting from the length resonances should disappear and, within the framework of such models, should lead to the observation of well quantized conductance plateaux, as shown in Fig. 20. At higher temperatures the broadening between conductance plateaux becomes significant as in the adiabatic model. At highly elevated temperatures $k_{\mathrm{B}}T > \Delta\epsilon_n(\sim \epsilon_{\mathrm{F}}/n)$ it is to be expected that the conductance quantization disappears completely. Whether or not such thermal effects are observed experimentally will depend critically upon the

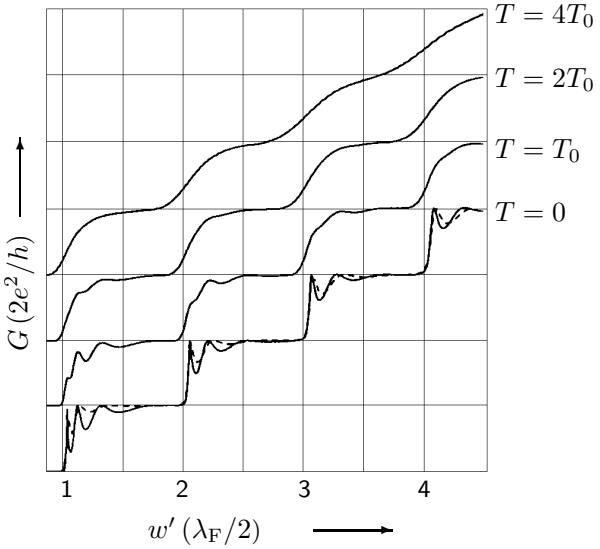

Fig. 20: The temperature dependence of the channel conductance in the WNW model [89S6] is shown as a function of the channel width. The parameter $T_0 = 0.02\epsilon_{\mathrm{F}}$ is chosen such that typical experimental data correspond to $T \approx 3T_0$. The dashed line shows the exact numerical result at $T = 0$.

temperature dependence of other system parameters in real devices. In particular the assumption of ballistic transport requires both elastic and inelastic scattering lengths significantly longer than the channel length. While the former is strongly dependent upon the material quality the latter exhibits a strong temperature dependence in semiconductors at low temperatures.

3.1.5 Sample geometry

The comparative robustness of the conductance quantization in high-mobility samples at low temperatures leads one to suspect that the sample geometry plays a subsidiary role in determining the conductance characteristics. Theoretically, this robustness can be understood within the adiabatic model if the channel length (i.e. the region over which the adiabatic separation is valid) exceeds a certain critical length, $L > L_{\mathrm{c}} = \sqrt{Rd_{\mathrm{c}}}$. Nevertheless the detailed form of the channel geometry may well be significant; a more rigorous analysis of the conditions under which a smooth channel variation can be expected to yield good conductance quantization has shown that the wavefunction matching between channel and reservoirs when adiabatic conditions break down is of the utmost importance [90Y1]. If the number of occupied transverse modes at this point is small compared with the total number the channel can theoretically accommodate then the matching is optimal

and the conductance quantization is good, even though mode conservation in the reservoirs is not given.

The simple adiabatic picture of quantum transport in QPCs has been extended [90G2], and the difference between local and global adiabatic regimes discussed. Within this picture the quantized conductance is a manifestation of local adiabaticity at the narrowest point of the constriction. However, mode conservation is not given throughout the device, and each QPC mode couples to many modes in the surrounding 2D reservoirs. Mode conservation over the entire device geometry, corresponding to global adiabaticity, is given only in the limit of a finite perpendicular magnetic field. The critical field necessary for global adiabaticity scales with the mode index and is approximately given by

$$B_n^{\text{global}} \approx 0.33\sqrt{n}\,\frac{\hbar k_{\text{F}}^2}{2e}\left(\frac{\lambda_{\text{F}}}{R}\right)^{3/2}\left(\ln\frac{2\pi R}{\lambda_{\text{F}}}\right)^{3/4} \tag{49}$$

in the low-field limit. Such global adiabaticity is particularly important for the explanation of the magnetic field dependence of the conductance quantization considered below.

For WNW models a clear quantization corresponds to an intermediate channel length which suppresses the tunneling of states above the Fermi energy but which is sufficiently short to prevent resonant effects resulting from the channel length. As discussed above [89S6] tapering of the WNW at the ends of the constriction does not signifcantly dampen the magnitude of the expected length resonances. However, a systematic theoretical study [91T] has shown that wedge shaped geometries provide for better quantization as the opening angle of the wedge increases (i.e. for point-like geometries) as shown in Fig. 21. For very sharp geometries the conductance quantization

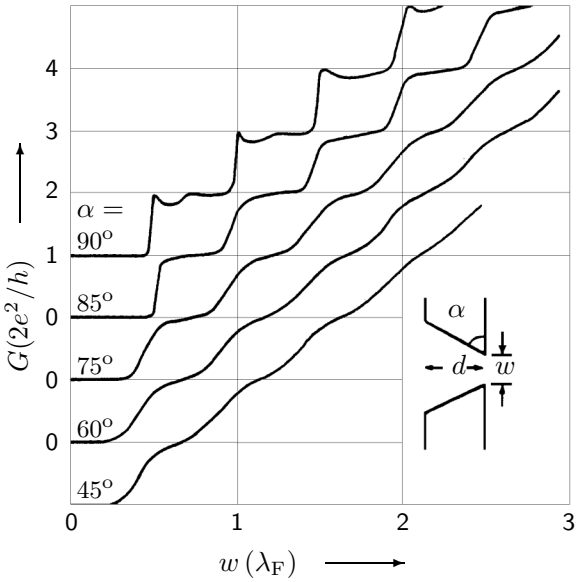

Fig. 21: The conductance $G(w)$ for wedgelike QPC geometries is plotted for various opening angles of the wedge as a function of the channel width [91T].

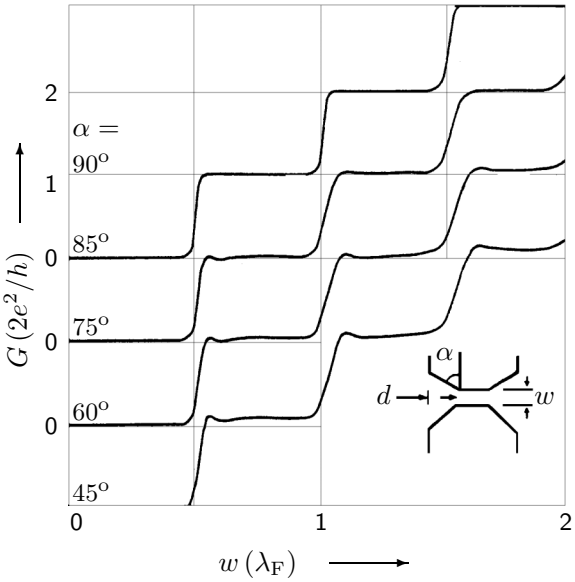

Fig. 22: The conductance $G(w)$ for tapered QPC geometries is plotted for different taper angles as a function of the channel width [91T].

weakens and a monotonic increase in conductance with QPC width is observed as discussed before [89H2, 89vdM]. Interestingly, analysis of the tapered geometries suggest that here also a small amount of tapering is sufficient to remove the length resonant structure (see Fig. 22) which then reappears as the tapering becomes more abrupt. This result is in contrast with previous work and it has been suggested [91T] that there exists an optimal opening angle between $85^{\text{o}} \leq \alpha < 90^{\text{o}}$ for the observation of conductance quantization.

The dependence of the quantization upon the channel size has been considered in a two-dimensional QPC where the active channel ranges from a mesoscopic wire to a single atom, the latter limit being of interest for the investigation of metallic QPCs [95M1]. With the WNW geometry assumed the essential features common to all such models are clearly reproduced.

Nonadiabatic models for the ballistic transport in mixed geometries, i.e. constrictions with a smooth but sharp geometry, have shown that the quantized conductance may still be theoretically expected, but that in such model systems the intermode mixing plays a significant role in the observation of well quantized plateaux [92C1]. The introduction of an effective potential with two maxima in the direction of the current flow leads to the expectation of resonant structure in the conductance if mode-mixing is neglected. Only when the non-adiabatic nature of such abrupt geometries is included through the mode mixing does the conductance become a smooth function of the Fermi energy with clearly defined plateaux.

A detailed comparison [94M] of the salient features of the various theoretical models has confirmed the robustness of the conductance quantization, and suggests that in realistic samples the quantization is better than that expected from the assumption of a purely local adiabaticity. Furthermore, it is shown that the supposed improvement upon local adiabaticity, the so-called diagonal approximation as discussed above [90Y1], can in fact show significant deviations from exact numerical calculations of the quantized conductance. Typical results are shown in Fig. 23; the diagonal approximation shows severe deviations from the other models and the best quantization is observed for the exact calculations. This effect is explained as an effective increase in channel length which leads to a smoothening of the abrupt channel geometry considered.

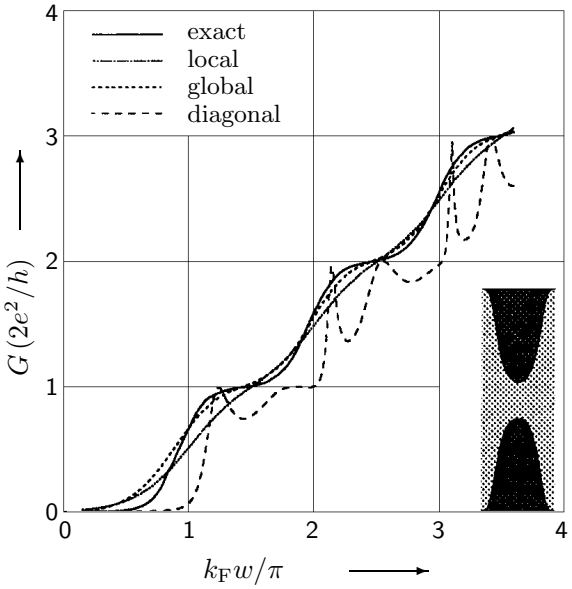

Fig. 23: The conductance is plotted as a function of the Fermi wave number for an abrupt QPC geometry. The figure compares an exact calculation (full line) with three common approximations [94M]. The inset shows the hard-walled geometry assumed for these comparative calculations.

An interesting modification of the standard QPC geometry is one in which the channel modes can couple via a tunneling barrier into a laterally defined reservoir [92T3]. In such a geometry the expected conductance quantization, with suitable modifications due to the hard WNW structure considered, has been calculated, and in addition the tunneling current which escapes sideways determined. It was found that the tunneling current depends upon the nature of the tunneling barrier between channel and lateral reservoir. The results of such calculations are summarized in Figs. 24 and 25 where both the channel transmission as well as the tunneling transmission are plotted as a function of subband index for two extreme cases. For a thin, high tunneling barrier (as shown in Fig. 24) the conductance quantization is accompanied by a tunneling current which decreases rapidly after the onset of transmission and resembles the k^{-1} behaviour of the 1D density of states. By contrast, Fig. 25 shows the situation for a broad but low tunneling barrier between QPC and reservoir. Both the direct transmission and the tunneling transmission

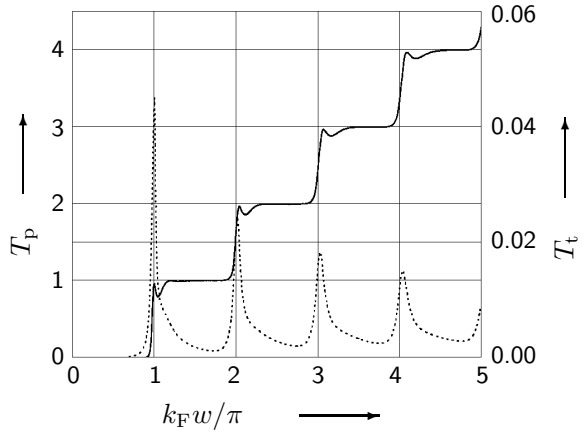

Fig. 24: The channel transmission probability T_p and the lateral tunneling probability T_t are shown as a function of channel index for $k_F d/\pi = 0.1$ and $U/E_F = 40$ corresponding to a thin, high tunneling barrier. [92T3].

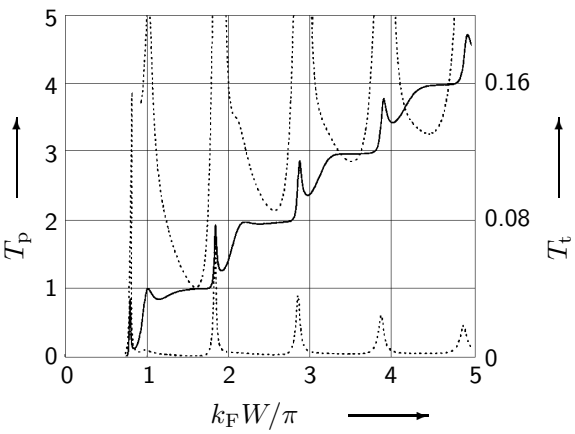

Fig. 25: As in Fig. 24 but for $k_F d/\pi = 1$ and $U/E_F = 1.8$ for a broad and low barrier [92T3]. The parameters U and d determine the height and width of the tunneling barrier.

show clear resonant structure below the onset of the actual quantized conductance. This can be attributed to the formation of weakly bound states within the QPC channel itself as a result of the relatively strong coupling to the tunneling reservoir.

3.1.6 Magnetic field

The application of a magnetic field perpendicular to the plane of the 2DEG leads to the formation of Landau levels in the bulk. Within the QPC itself the lateral quantization arising from the narrowness of the channel will be modified by this addditional magnetic quantization, and hybrid magneto-electric subbands are expected to form when the cyclotron radius $l_c = \hbar k_F/eB$ becomes comparable with the channel width. The number of occupied subbands is now also dependent upon magnetic field and allows simple models for the lateral confining potential to be compared [88B2], and important parameters such as channel width and electronic density within the channel to be determined. The deviations from a linear depopulation with inverse magnetic field are an essential characteristic of one-dimensionality, both for long 1D channels as well as for QPCs. In QPCs this results in a modified characteristic of conductance with channel width; both the conductance plateaux as well as the steps between them become better defined as a function of the channel width with increasing magnetic field. Within the context of the adiabatic model the effect of a perpendicular magnetic field has been calculated using perturbation theory. Both the conductance plateaux width (measured as a function of channel width) as well as the step size between plateaux increase quadractically with magnetic field [89G2] for small field strengths. Furthermore, the spin-degeneracy assumed for the lateral quantization within the QPC in the absence of a magnetic field, will be lifted regardless of field orientation. This effect can be best observed in a parallel configuration [88W1] where the influence on the lateral quantization is minimal. In such a configuration the magnitude of the spin-splitting has been shown [89G2] to scale linearly with magnetic field and with plateau index. This leads to the expectation that spin-split plateaux can be observed only for high-index plateaux with

$$n > n_c = \left(\frac{2}{\pi}\right)^2 \left(\frac{\lambda_F}{R}\right) \left(\frac{E_F}{g\mu_B B}\right)^2 \tag{50}$$

at high fields.

The conductance and thermopower of a ballistic QPC have been considered [92P1] in a WNW geometry at high magnetic fields. It is found that increasing the magnetic field leads to an improved quantization and to less pronounced resonant structure resulting from the channel length. The oscillatory behaviour of the thermopower is enhanced by the application of the magnetic field and the oscillations become markedly asymmetric with significantly larger positive contributions.

Another fundamental aspect of 1D ballistic transport in the presence of a magnetic field is the nature of the Hall effect. This question was addressed initially in cross-type geometries consisting essentially of two QPCs in series. The fundamental experimental result is the observation of a Hall voltage close to zero for finite magnetic fields [87R]. Although the origin of this so-called "quenching" was initially hotly contested [88K1, 89K4] the currently accepted explanation is based upon a simple model of collimation in QPCs [89B2], which is of relevance to many other transport phenomena. Within the framework of the Landauer-Büttiker formulation of transport in mesoscopic devices the Hall resistance R_H can be written in terms of the transmission probabilities,

$$R_H = \frac{h}{e^2} \frac{T_R - T_L}{2T_F(T_F + T_R + T_L) + T_R^2 + T_L^2} \tag{51}$$

where T_L, T_R, and T_F correspond to the transmission coefficients to the left, right and forward directions in the cross geometry, respectively. Clearly, the observation of zero Hall voltage necessarily requires that T_L and T_R are identical, but makes no statement as to their absolute magnitude. In fact the accepted picture is that both T_L and T_R are almost zero, and that the observation of a generic quenching of the Hall effect can be only explained in terms of the broadening of the QPC constrictions at the entrance and exit as discussed in the adiabatic models (or WNW with taper) above [89B2]. In such channels the gradual decrease in lateral quantization energy is associated with the simultaneous growth of the momentum along the channel. Thus a QPC focuses the electronic trajectories emanating from the QPC in the forward direction in much the same way as a trumpet focuses sound. This collimation is of importance in understanding both the coherent electron focusing experiments [88B1] which motivated the initial QPC investigations, as well as the non-additivity of QPC resistances [88W2, 89B3].

In electron focusing experiments electrons injected through a point contact are, in the presence of a perpendicular magnetic field, focused towards a collector contact, whose voltage serves as a measure for the number of electrons arriving at the collector. Semiclassically, the ballistic injection of electrons gives rise to a periodic focus condition for multiples of the magnetic field $B = 2\hbar k_F/eL$ where L is the lateral separation of the injector and collector contacts [88B1], and consequently to the observation of periodic oscillations in the measured collector voltage. In QPCs at low temperatures deviations from such behaviour are observed due to the coherent excitation of the magnetic edge states occupied at the sample edge. Quantitative calculations of the expected probability density at the collector contact show significant deviations from the simple periodic behaviour as shown in Fig. 26.

In strong magnetic fields near filling factor $\nu = 1/2$ the behaviour of a 2DEG can best be described in terms of so-called composite fermions (CFs). These quasiparticles, consisting essentially of two flux quanta associated with each electron in the 2DEG, move within the mean-field generated by the spin-polarized electrons and the external field. For $\nu = 1/2$ the mean-field for the CFs is zero and many phenomena which are observed at zero field for 'free' electrons are expected to be visible for their composite counterparts. The conductance quantization for ballistic CFs is however modified due to the subtle interplay between mean magnetic field and electron density. Simple models of ballistic QPCs in the high-field limit suggest that the non-uniform electron density within the channel leads to a non-zero mean magnetic field and the expected conductance quantization has been predicted to be visible [96K3] only for filling factors $\nu > 1/2$. This strikingly nonmonotonic behaviour leads to the variation of conductance quantization shown in Fig. 27 where an abrupt drop in the conductance associated with the filling factor $\nu = 1/2$ is clearly visible.

The transport properties of a ballistic channel in the presence of a parallel magnetic field oriented along the direction of current flow have also been investigated [93B]. The magnetic

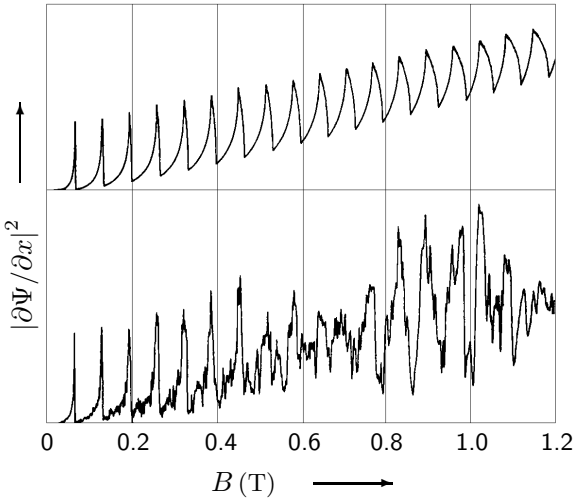

Fig. 26: The calculated electronic probablility density at the collector expected in electron focusing experiments is shown as a function of perpendicular magnetic field [88B1]. The lower trace shows the result when phase coherence between the edge states is assumed, while the upper trace demonstrates the incoherent case.

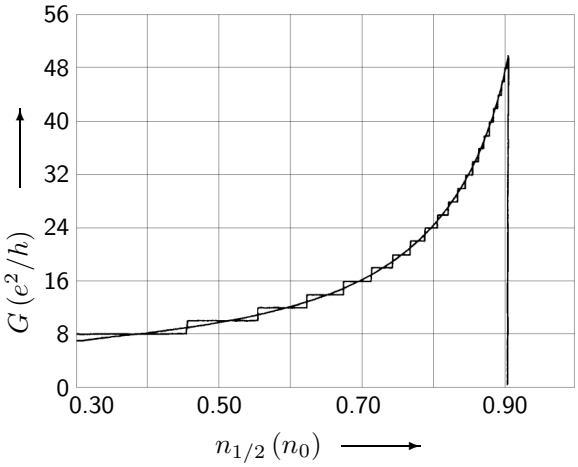

Fig. 27: The conductance quantization of a ballistic QPC in the high-field 'composite fermion' limit is shown as a function of the parameter n_0 related to the electron density within the constriction which scales with perpendicular magnetic field [96K3].

field dependence of the laterally quantized states leads to fluctuations in the number of occupied channels for weak magnetic fields. The appropriate magnetic field strength is given by the flux neccesary for a shift in energy levels of the order of the average level spacing, $E_F/(k_F a)^2$ with a the channel radius, and is thus predicted to be a small fraction of the flux quantum $\phi_0 = h/e$ for a quasi 3D channel. Although the geometry considered was a long ballistic channel the essential conclusions could presumably also be valid for ballistic QPCs defined in the appropriate system, i.e. with comparable quantization energies in both lateral directions.

The observation of periodic structure in the magnetoresistance of some ballistic QPCs has prompted theoretical calculations [94MR] which suggest that this structure may in fact be related to the creation and annihilation of vortex-antivortex pairs, in contradiction to the generally accepted interpretation of Aharonov-Bohm (AB) type oscillations. It is argued that the closed path required for AB-oscillations is highly unlikely due to the suppression of backscattering in a magnetic field, and that the observed oscillations are associated with the trapping of vortices under the potential barrier created by the QPC. Such effects are expected to be most pronounced as the subbands switch into the conductance.

3.1.7 Impurities

Although the conductance quantization is a manifestation of 'perfect' transmission, a QPC is an inherently mesoscopic device and it is therfore to be expected that disorder will play a role in the determination of the individual device characteristics. The naïve expectation that the

impurity configuration in the immediate vicinity of the QPC will produce a characteristic device 'fingerprint' has indeed been theoretically confirmed. The tight-binding Hamiltonians discussed above [89M, 89H2, 89vdM, 89H3, 93H1] are particularly amenable to such theoretical investigations, and several new effects resulting from disorder have been predicted. For an ensemble of QPC devices [89M] the conductance is predicted to no longer be well quantized in the presence of weak disorder, here included as a fluctuation of the local site energies within the channel. The characteristic equidistant steplike structure of the conductance plateaux should still be observed but with a stepsize which decreases linearly with increasing disorder. Furthermore the disorder is predicted to induce mixing between subbands; as a result the occupation of localized states at the band edge of higher subbands can mix with conducting states of lower subbands. As a consequence a resonant decrease in the conductance is predicted as each subband is tuned below the Fermi energy. The mesoscopic character of QPC devices is most clearly demonstrated in the tight-binding calculations with a single impurity state [89H2, 89vdM] whose position relative to the QPC constriction is systematically varied (see Fig. 28). Both a qualitative reduction of the conductance

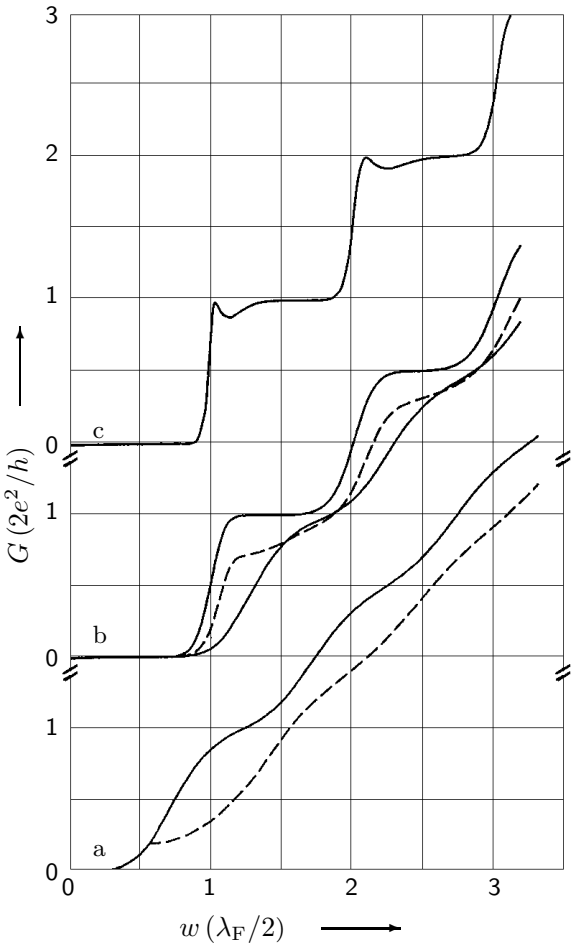

Fig. 28: The QPC conductance as a function of channel width for various impurity configurations; a) channel with and without impurity, dashed and full line respectively for $L = 0$, b) channel without impurity ($L = 0.48\lambda_F$) - upper solid curve, impurity in channel ($x = 0.32\lambda_F, y = 0.32\lambda_F$) - lower solid curve, impurity outside channel ($x = 0.57\lambda_F, y = 0.32\lambda_F$) - dashed curve, c) channel without impurity, channel length $L = 0.99\lambda_F$ [89H2].

plateaux as well as a quantitative reduction of the quantized values are clearly observed. This very general observation has been confirmed [89H3, 93H1] in other tight-binding calculations where the transition to universal conductance fluctuations (UCFs) for strong elastic scattering is predicted. Similarly the presence of inelastic scattering will also destroy the conductance quantization and, in the absence of coherent transport, lead to a smooth, monotonic variation of conductance. Even if no impurity is to be found in the immediate vicinity of the QPC, disorder within an inelastic scattering length of the constriction will yield a mesoscopic correction to the conductivity. In bulk samples such UCF conductivity corrections are generally of the order of e^2/h which is comparable

to the conductance of the QPC itself. However, such fluctuations are not seen in the conductance of a QPC due to the filtering action of the channel modes [93M2]. Any fluctuations of the surrounding diffusive region are suppressed by a factor of $2(n/N)$ where n is the number of channel modes and N the number of modes in the reservoir within an inelastic scattering length of the constriction.

The lack of good quantization in channels whose length is considerably shorter than the elastic mean free path in high quality heterostructures has led to investigations of the role of the random impurity potential generated by the donors in the dopant layer [91N, 91L1]. The donors are assumed to be fully ionized and distributed randomly throughout the dopant layer, while the 2DEG is treated as an infinitely thin sheet whose electron density is given by the local potential within the sheet. Qualitatively, it has been found that whilst good quantization is found in short QPC devices, even devices whose length is considerably smaller than the elastic scattering length show strong deviations from quantized behaviour [91N]. Typical electronic density profiles are shown in Fig. 29 where the parameters of the model have been chosen to simulate realistic device geometries. These simulations suggest that good quantization is obtained when the channel length

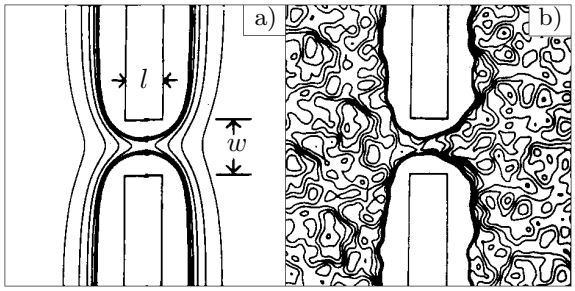

Fig. 29: The electronic density in the vicinity of a QPC device is shown for a realistic device geometry both a) without and b) with the influence of the random dopant potential included [91N]. The contours are for constant electron density.

is shorter than the correlation length of the random impurity potential, and that significant, sample specific deviations are to be expected resulting from the impurity configuration in the immediate channel vicinity. This analysis has been extended to consider the role of intermode scattering [91L1] in the presence of a random impurity potential. It has been shown that the adiabatic approximation does not hold in this limit, and that rapid intermode scattering will occur. Nevertheless, conductance quantization can be expected for short channel geometries due to the predominantly forward nature of the scattering. Related calculations [95Z], performed with realistic impurity potentials, have stressed the importance of quasi-localized states at the Fermi energy which can lead to indirect backscattering and hence to a loss of quantization. The breakdown of the conductance is quantified in terms of its deviation from ideal quantization, and the statistics of these fluctuations are calculated for an ensemble of QPCs. The probability distribution for such realistic geometries follows the from of a generalized Poisson distribution.

The effect of impurity scattering has also been investigated for adiabatic QPC models [94C, 94K1]. For the saddle point constriction considered above [90B2] an attractive impurity located at the centre of the constriction leads to a loss of quantization and to the presence of additional resonant structure at the onset of conduction for each subband. Interestingly, an attractive potential located outside of the QPC itself can give rise to additional resonant structure, which results in an increased conductance as shown in Fig. 30; an effect which has been also been predicted for simple WNW geometries [90T1]. Similar results have been obtained [94K1] for the hyperbolic confining potential discussed previously [89K1].

3.1.8 Interactions

The electronic transport in an interacting electron system in the one-dimensional limit has been extensively investigated theoretically. In the context of ballistic QPCs the question of whether the quantized conductance should be renormalized as a consequence of the interactions has been the subject of much debate. For the case of a perfect 1D wire with a tunneling barrier located

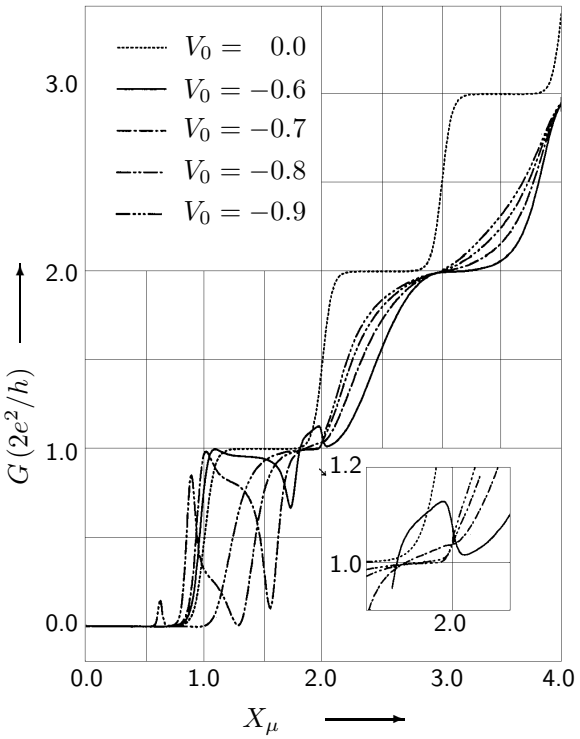

Fig. 30: The conductance of a saddle-point QPC with an additional attractive impurity located in the lateral parabolic potential is shown as a function of the QPC width. The inset illustrates the increase in conductance which can occur in the presence of an attractive impurity [94C].

somewhere along its length, the conductance as a function of transmission coefficient t and interaction parameter g has been calculated for the various interacting regimes [92K]. For repulsive interactions ($g < 1$) it has been found that the $T = 0$ limit of zero conductance vanishes according to the power law

$$G \sim t^2 T^{2/g-2}, \tag{52}$$

while for attractive interactions ($g > 1$) the zero temperature conductance should scale according to $G = ge^2/h$ for all nonzero t for spinless fermions. Additionally, the interacting regime should manifest itself in deviations from the otherwise linear, ohmic behaviour with a current-voltage charateristic given by the power law $I \sim V^{2/g-1}$ for voltages above a critical voltage $V_L = \hbar v_\mathrm{F}/eL$ where L is a length scale over which the electronic interactions are assumed to operate. In the case of a ballistic QPC this may be identified with the channel length since the source and drain reservoirs are invariably two-dimensional and can thus be treated as a Fermi liquid.

Comparable results have been derived by other authors [95F] and the theoretical models have also been extended to include the effects of high magnetic fields. In particular, exact nonequilibrium solutions for the transport properties of QPC devices in the fractional quantum Hall regime have been derived [95F], and predict similar power law behaviour for both the current-voltage characteristics as well as for the tunneling conductance versus temperature.

More recently however, the prediction of a renormalized quantized conductance has been called into question for the case of an ideal QPC [95M2, 95P, 96K2, 96O, 96A] or equivalently a ballistic 1D channel, connected to reservoirs. All of these theoretical treatments stress the role of the reservoirs to which the QPC is attached and show that the predicted renormalization is in fact an artefact resulting from the assumption of purely 1D Luttinger liquid behaviour along the entire device length. In any realistic device geometry the interacting 1D channel will inevitably open out into reservoir regions where the potential drop is actually measured. Treating these reservoir regions as Fermi liquids [95M2, 96A], or as non-interacting 1D regions [95P], the usual quantized result is recovered. Other approaches [96K2, 96O] have emphasized the renormalization of both the chemical potential, as well as current, within the 1D channel. Although both are influenced by the interactions, the channel conductance, defined essentially as the ratio of the current to the

potential drop remains unaffected.

3.1.9 Electron spin

Self-consistent calculations of the electronic structure in one-dimensional channels in a parallel magnetic field have been performed [96W] in an attempt to model some of the more recent experimental results on very high-mobility QPC samples. Using spin-polarized density functional theory it was shown that the exchange interaction causes a significant subband splitting as the Fermi energy passes through the subband structure, and that this effect can occur also at zero magnetic field. This effect could explain the observation of additional conductance features below $2e^2/h$ and it is conjectured that such anomolous conductance features might also be visible for higher subband occupancy.

3.1.10 Non-linear effects

The simplest treatment of non-linear effects in QPCs assumes a prefectly symmetric voltage drop along the length of the QPC channel [88G1, 89G1] within an adiabatic model. As discussed above the energy scale relevant to the onset of conduction for a particular channel mode n is given by

$$\Delta_n = \frac{n\hbar^2}{m\sqrt{2Rd_c^3}}. \tag{53}$$

When a finite bias is applied to the reservoirs connected to the channel the occupation of reservoir states is assumed to be modified accordingly. The shifts in electrochemical potential, $(\pm eV/2)$, are also reflected in the occupation of the channel modes and hence the total transmitted current. This leads to an effective broadening between the conductance plateaux at finite bias and eventually to the disappearance of the conductance plateaux when the energy spacing between quantized levels becomes comparable with the applied bias. Interestingly these models also predict the emergence of additional quantized steps in the differential conductance at intermediate values of conductance $G = (2n-1)e^2/h$ for low index plateaux in the voltage range $n < 2E_F/eV$. This behaviour is illustrated in Figs. 31 and 32 as a function of the continuous dimensionless parameter $z = k_F d/\pi$ which defines the number of occupied subbands, and reflects the assumption of a symmetrical voltage drop along the channel length. If this assumption is relaxed then the additional plateaux structures are still predicted in the non-linear regime but are no longer perfectly quantized. Rather the observed differential conductance for the lowest conductance plateau is predicted to be given by $G = \beta 2e^2/h$ and $G = (1-\beta)2e^2/h$ where β is the fraction of the potential dropped at the entrance to the ballistic channel [89K6].

The above model has been extended to include the effects of a magnetic field and, in addition, the effect of a non-linear variation of potential drop within the channel, i.e. for $\beta = \beta(V_{sd})$ [92MM]. The magnetic field lifts the spin degeneracy of the subbands and results in the observation of additional quantized plateaux in the linear response limit. In the non-linear regime the same qualitative picture can be applied as above and gives rise to additional plateaux with quantized conductance $G = (n+1/2)e^2/h$ for the symmetric case, or more generally to plateaux $G = (n+\beta)e^2/h$ and $G = (n+1-\beta)e^2/h$. When the electric field distribution within the QPC becomes a function of the applied voltage itself then the steps in the differential conductance are no longer well quantized, but shift with the applied bias. For the case of a parabolic variation of the voltage drop, the observed steps manifest a linear slope.

The effect of coherent mode-mixing on the non-linear conductance of QPC devices has been considered [94Z], and it is suggested that nonlinearities, even at extremely small applied source-drain bias $eV_{sd} \ll \Delta E$, can occur. Although mode mixing is believed to play a relatively insignificant role in the conductance quantization due to the fact that the weak scattering potentials in QPC systems produce no backscattering, under certain circumstances conductance corrections can occur as a result of mode interference. In an adiabatic constriction with two isolated scattering centres the

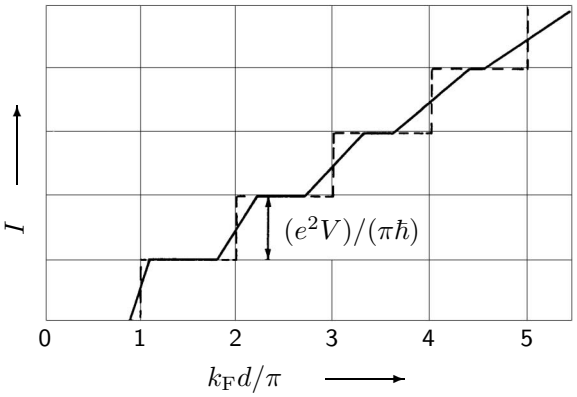

Fig. 31: The current in units of $e^2V/\pi\hbar$ is plotted as a function of the dimensionless parameter $z = k_F d/\pi$. The smearing of the quantized steps at finite voltage (full line) is compared with the $V = 0$ result (dashed line) [89G1].

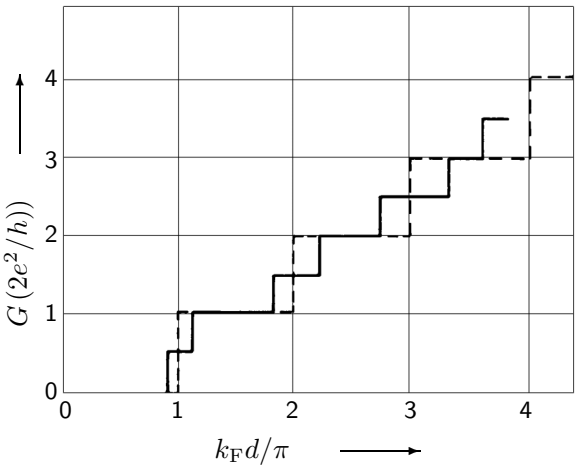

Fig. 32: The emergence of additional quantized steps in the differential conductance is plotted as a function of the dimensionless parameter $z = k_F d/\pi$ [89G1].

phase difference between two partial waves, propogating in different channel modes is sensitive to the potential along the channel, as in the electrostatic Aharonov-Bohm effect. The linear response conductance is, as a consequence of unitarity, unaffected, however the differential conductance is predicted to show small (a few %) corrections, which are also manifest in the rectified response of the QPC device.

Landauer's conductance formula has been extended to include the case of finite voltages and finite temperatures [89B1] where, under the assumption of ideal conductance in the reservoirs connected to the QPC, the current I flowing can be shown to be a convolution of the form:

$$I(E,V,\theta) = \frac{e^2}{\pi\hbar}\,T(E,V) * [\Theta(E+eV) - \Theta(E)] * \left[-\frac{\mathrm{d}f(E,\theta)}{\mathrm{d}E}\right]. \tag{54}$$

The convolution can be intuitively seen to depend upon the energy and voltage dependent transmission coefficient, as well as upon both the finite voltage V and the derivative of the Fermi distribution function $f(E,\theta)$. Cast in this form the broadening between quantized conductance plateaux associated with an increased temperature is clearly independent of the broadening connected with a finite voltage in the non-linear regime.

The assumption of a symmetric voltage distribution along the channel length, while convenient for model calculations, is presumably only reasonable for small deviations beyond the linear response regime. As suggested in the phenomenological models above [89K6, 92MM] the potential distribution is generally expected to be asymmetric and indeed to be a function of the applied bias. For finite voltages a non-uniform electronic charge density along the channel evolves which will screen the external field. A self-consistent solution of the Poisson equation for a QPC geometry then leads to an integrodifferential equation for the potential distribution in the QPC [89L1], which can only be solved exactly for the simplest of cases. Qualitatively, it is be expected that the potential drop along the ballistic QPC channel is concentrated at the entrance and exit to the channel. Under high-bias conditions the associated space-charge build-up has been predicted to lead to current instabilities [92F2, 92F1] which, due to the short transit time for electrons in the channel, could lead to interesting high-frequency behaviour.

A simpler model for the transmission in the high-bias regime neglects the space-charge build-up and also assumes that the channel transmission is non-adiabatic [89K3, 89K2]. Calculations of the

energy dependent transmission coefficients suggest that the non-linear characteristics are modified due to a significant reduction of the transmission, and predict that the high-bias characteristics should manifest a pronounced negative differential conductance. In conjunction with other device parameters, such as the small channel capacitance in the tunneling regime and the transit time for ballistic electrons, this has led to the suggestion that QPCs are interesting candidates for future high-frequency devices.

3.1.11 Series configurations

As discussed above in the case of low-field Hall measurements, it has been predicted that the inevitable tapering at the exit of a QPC will lead to a collimation of the transmitted electrons. This suggestion has motivated the experimental and subsequent theoretictal consideration of a series configuration of two QPCs with separation smaller than the scattering length. The conductance of this series configuration will deviate from that expected for purely ohmic transmission, and in the limit of perfect transmission through the series geometry the measured conductance would be given by the quantized conductance as in the simple QPC geometry. In a realistic QPC geometry both the channel tapering and any potential step at the exit of the QPC will lead to collimation effects and hence to a modified series conductance. These effects have been modelled [89B3] and the conductance can be shown to be given by:

$$G_{\text{series}} = \frac{1}{2} G_0 \left(1 + \frac{f W_{\max}}{2L} \right) \tag{55}$$

where G_0 is the conductance of the individual QPCs (measured separately), $W_{\max}$ the channel width at the exit (entrance), L the channel length and $f = f_{\text{b}} f_{\text{t}}$ is the collimation factor resulting from both barrier collimation and tapering. The latter is essentially given by the channel geometry $f_{\text{t}} = W_{\max}/W_{\min}$, while the former is related to the potential step E_0 at the constriction exit via $f_{\text{b}} = (1 - E_0/E_{\text{F}})^{-1/2}$. A quantum-mechanical calculation for the series geometry [92T2] has reproduced the important features of the above model and has also extended the analysis to include an asymmetric tuning of the individual QPCs. In this limit it is shown that the conductance is determined by the narrower QPC, i.e. the QPC with lower conductance. Furthermore, for a series configuration of QPCs with additional lateral confinement between the QPCs a transmission resonance originating from bound states is predicted. The parity of this state and its consequent coupling to the QPC modes strongly influence the conductance, and both an enhanced as well as a reduced transmission have been derived. The angular distribution of electronic transmission through series QPC configurations has been considered [92S2] within a quantum mechanical diffraction model, which extends the semiclassical picture of collimation discussed above. Typical

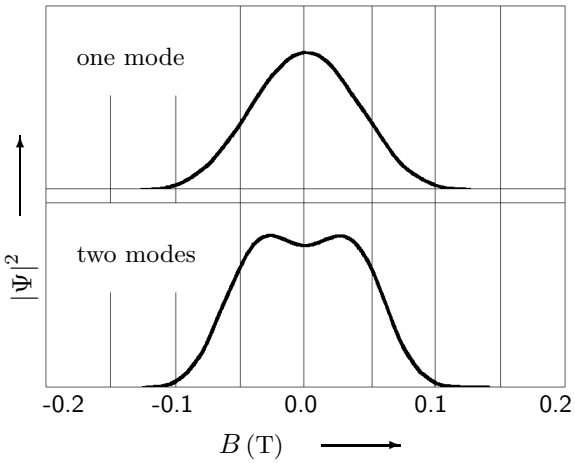

Fig. 33: The calculated probability density for the detection of electrons in a collimation geometry [92S2] is plotted as a function of the applied magnetic field. The two traces correspond to the situations when different numbers of subband modes within the QPC are occupied.

results are illustrated in Fig. 33 and demonstrate that both the collimation resulting from the

geometrical tapering as well as diffraction of the electron waves at the exit should be present in the transmitted electron beam. Subsequent numerical analysis [94U] has stressed the importance of wedge shaped QPC geometries in attaining good collimation at the detector QPC.

3.1.12 Electromagnetic environment

The modification of the quantized conductance resulting from the interaction of the surrounding 2D reservoirs with a resistive electromagnetic environment [92H2] has been considered, and a reduction of the low-voltage conductance predicted. For an adiabatic channel the traversal time over the adiabatic regime $\tau_{\mathrm{trav}} = \sqrt{dR}/v_{\mathrm{F}}$ defines a cut-off frequency for the fluctuations of the environment. For a sufficiently resistive environment the evolution of a current blockade is predicted for a conducting geometry even in the absence of any capacitance as shown in Fig. 34. The gap is given by $V_{\mathrm{gap}} = eR_{\mathrm{E}}/\pi\tau_{\mathrm{trav}}$ where R_{E} is an impedance given by the fluctuating environment.

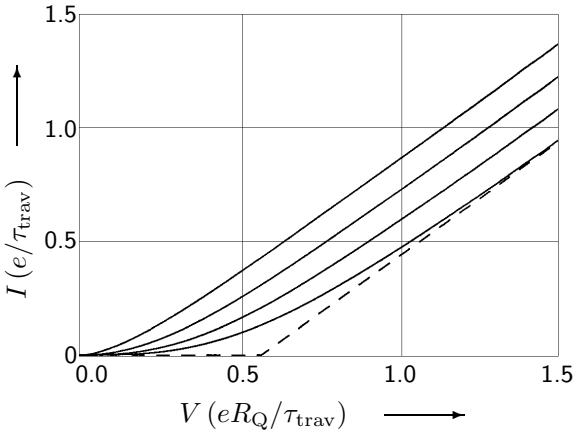

Fig. 34: The current-voltage characteristics for a QPC in a resistive electromagnetic environment are shown for different ratios of environmental resistance R_{E} and QPC resistance R_{Q} (here taken to be ideally $h/2e^2$) and for traversal time τ_{trav}. The values $R_{\mathrm{E}}/R_Q = 0.5, 1.0, 1.5, 2.0$ are shown, the dotted line extrapolates the high-field ohmic behaviour for the case $R_{\mathrm{E}}/R_{\mathrm{Q}} = 2.0$ [92H2].

The quantum-mechanical nature of a ballistic QPC is reflected not only in the quantization of the conductance but also in the quantization of other system parameters. For example the low-frequency admittance gives information about the capacitance of a QPC [96C]. By virtue of their small density of states, mesoscopic devices are expected to show significant deviations from the capacitance as defined purely by the geometry of the device. Furthermore, for a system with finite conductance there is a distinction between the static and dynamic properties. To accommodate this distinction a device emittance

$$E = i\left(\frac{\mathrm{d}G}{\mathrm{d}\omega}\right)_{\omega=0} \tag{56}$$

is defined which can then be related to the reflection and transmission coefficients of the QPC. The theoretical results for a QPC with the saddle-point geometry discussed above [90B2] are shown in Fig. 35.

3.1.13 Thermal transport properties

The transition region between quantized plateaux, is accompanied by oscillations in the thermopower of the QPC [89S5, 91P3]. The thermopower $S(\mu, T)$ is related to the transmission coefficients for the QPC modes T_i through an equation of the form:

$$S(\mu,T) = \frac{k_{\mathrm{B}}}{e}\frac{\sum_i \int_0^\infty \mathrm{d}E(-\mathrm{d}f/\mathrm{d}E)T_i(E)(E-\mu)/k_{\mathrm{B}}T}{\sum_i \int_0^\infty \mathrm{d}E(-\mathrm{d}f/\mathrm{d}E)T_i(E)}. \tag{57}$$

The resultant thermopower is quite generally expected to show oscillations as a function of the chemical potential, with maxima arising whenever a resonance with a subband energy occurs, the width of such oscillatory structure given by the energy scale on which the subband switches into

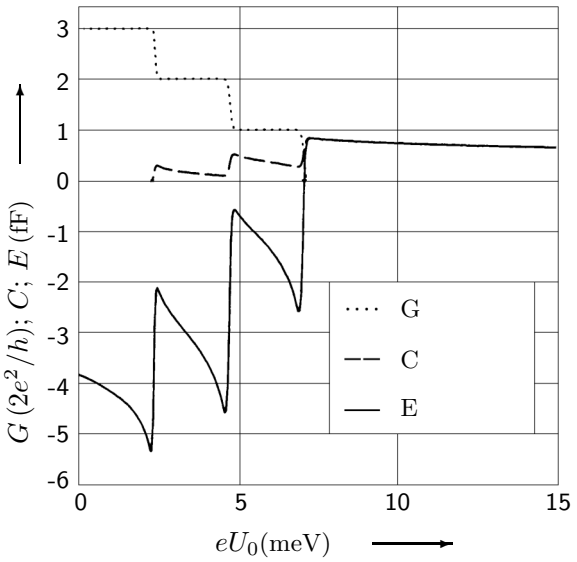

Fig. 35: The conductance (in units of $2e^2/h$; dotted curve), capacitance, and emittance (in units of fF, dashed and full curves) for the saddle point QPC geometry as a function of barrier height eU_0 at the entrance to the QPC with initially three conducting channels [96C].

the conductance. This behaviour is illustrated in Fig. 36 for the adiabatic confining potential considered above [90B2] with $\omega_y/\omega_x = 3$. At low temperatures $k_\mathrm{B}T < \Delta E_n$ the thermopower is predicted to show temperature independent local maxima with heights

$$S_n^{\max} = -\frac{k_\mathrm{B}}{e}\frac{\ln 2}{n+1/2} \approx -\frac{60}{n+1/2}\,\mu\mathrm{VK}^{-1}. \tag{58}$$

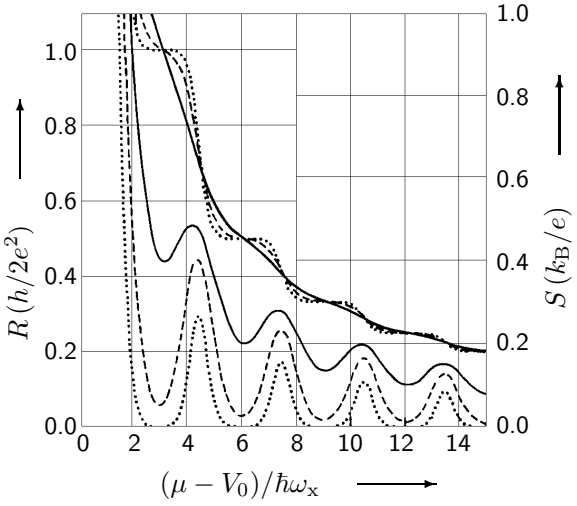

Fig. 36: The resistance and thermopower of a ballistic QPC are plotted as a function of the chemical potential for three different temperatures [91P3].

The influence of the electron-phonon interaction upon the quantized conductance of a ballistic QPC has been investigated [97C], and it was found that high-energy LO phonons should reduce the value of quantized conductance below $n(2e^2/h)$, while low-energy phonons can in fact enhance the transport along the channel and hence lead to an increased conductance. Furthermore, the conductance plateaux show additional structure which detracts from the quality of the quantization. These calculations were performed for significantly higher temperatures (30 K) than are usually employed in studying QPCs and also assumed Fermi energies an order of magnitude greater than is found in the semiconducting samples discussed here.

3.1.14 Superconducting weak links

The electronic transport in superconducting quantum point contact geometries has also been considered and predicted to have interesting quantized properties [91B1, 92F3]. For the case of a superconducting weak link whose length is shorter than the coherence length of the bulk material it has been predicted that the critical current becomes quantized according to $I_c = Ne\Delta_0/\hbar$, where Δ_0 is the energy gap of the bulk material and N may be identified with the number of propogating transverse modes within the QPC [91B1]. This result is however only valid providing the QPC channel length is shorter than the coherence length of the superconductor. For longer channels [92F3] the predicted steps will decrease in height from the above result, and scale roughly with the inverse channel length or rather the separation between the two superconducting regions of the device. As in the case of non-adiabatic transmission, the critical current can also develop resonant structure, which is correlated to the resonant structure in the conductance, as a result of length resonances occuring in abrupt WNW geometries.

3.2 Quantization

The observation of a conductance quantized in units of $2e^2/h$ is the most fundamental result associated with the transport properties of ballistic QPCs [88vW1, 88W1]. These first experiments were performed using lithographically defined gate electrodes to define a short, narrow constriction in the plane of a two-dimensional electron gas (2DEG) as detailed in Section 2.2 above. The application of a low-frequency current of sufficiently small amplitude and the phase-sensitive detection of the resulting voltage signal provides a direct measurement of the low-temperature sample resistance. Inevitably, even in a four-probe measurement configuration, an additional series resistance from the surrounding diffusive reservoirs must be subtracted from the measured resistance before the conductance quantization can be clearly discerned. In high-mobility samples at low temperatures however the magnitude of this correction can be smaller than 100 Ω and hence considerably smaller than the quantized conductance. Typical results are shown in Figs. 37 and 38 where the measured resistance and the extracted conductance of typical ballistic QPCs are shown respectively.

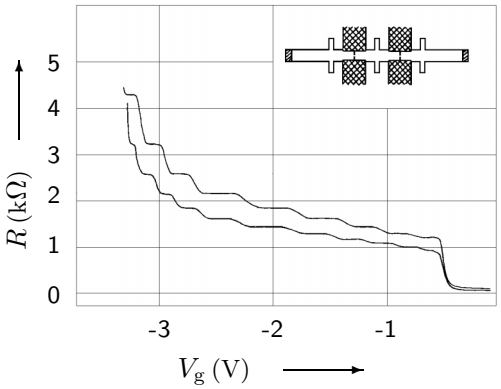

Fig. 37: The channel resistance at $T \sim 0.1$K is plotted as a function of the applied gate voltage. The two traces show results for different electron densities induced by illumination [88W1]. The inset schematic shows two QPC devices, with length and width of 400 nm and 500 nm respectively.

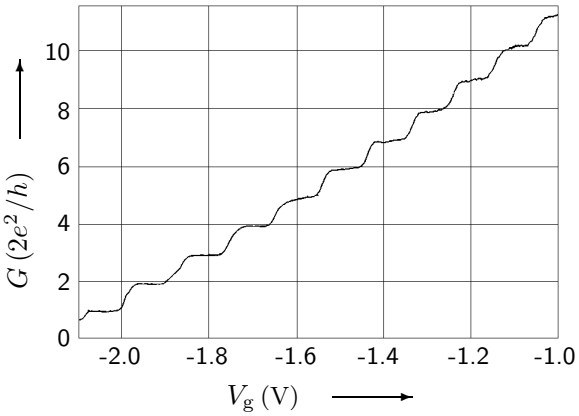

Fig. 38: The low-temperature conductance of a typical ballistic QPC is plotted as a function of the applied gate voltage after subtraction of the series resistance [88vW1]. The quantization of the conductance in units of $2e^2/h$ is clearly manifest.

In both of these original publications the Fermi wavelength λ_F was of the order of 40 nm and the channel width at defintion presumably 200 – 300 nm wide. The maximal number of trans-

verse modes thus defined is expected to be $n_{max} = 2W/\lambda_F$ roughly 10 – 15, in good agreement with the experimental observations. Thus, despite the obvious lack of translational invariance along the channels, the explanation of the quantized conductance in terms of the formation of one-dimensional subbands was postulated and widely accepted. Furthermore, the short channel geometry of the QPCs is essential for ballistic transport in the QPC itself. In GaAs/AlGaAs heterostructures the low-temperature elastic mean-free path ℓ_e can become as large as 10 μm; empirically the observation of a quantized conductance requires $\ell_e \gg L$ where L is the channel 'length'. Prior experiments in high-mobility 2DEG material with channel lengths as small as 5 μm [86T], demonstrated a clear one-dimensionality in the gate voltage dependence of the observed Shubnikov-de Haas (SdH) oscillations but no evidence for quantized conductance was seen.

In the above experiments the variation of channel width with applied gate voltage is approximately linear, and hence the number of modes in the conductance scales accordingly. A simple analytical model [89S1], based upon an electrostatic solution of an idealized QPC geometry with translation invariance in the current direction, predicts that the number of occupied subbands should scale according to

$$n(V_g) \propto (V_g - V_{po})^{\lambda} \tag{59}$$

where $\lambda \geq 3/4$ and V_{po} is the gate voltage at pinch-off. The weak deviation from linearity predicted is indeed qualitatively seen in the data; more detailed comparisons between experiment and theory are considered in Section 3.5 below.

As mentioned above the first observation of a 'quantized' step in conductance [87G] was seen in the abrupt change of the tunneling current of an STM contact and a metallic surface. However the observed quantization was poor, and furthermore only a single step at the onset of the conducting regime was observed. In contrast the quantization in semiconducting QPCs, while clearly not as good as that observed in the quantum Hall effect, can approach 0.1 % of the expected values. Subsequently good quantization has been observed in quantum wire devices [98K], and in metallic point-contacts [95K, 96K1]. Although many experimental aspects of the conductance quantization in metallic systems are comparable with those of semiconductor QPCs there are significant differences related to the differing energy scales and length scales. A discussion of the metallic systems is however beyond the scope of this survey.

Subsequent to the observation of quantized conductance in semiconductor QPCs and other metallic systems, a number of quantized analogies have been suggested and investigated [91M, 99T]. The optical analogue has been found in transmission experiments through a 2D slit when exposed to diffuse illumination of wavelength $\lambda = 1.55\,\mu$m. As the slit width was continuously increased the transmitted power rose in a stepwise fashion every time the slit-width changed by $\lambda/2$. Since the transmitted power is given by the transmission cross-section per unit length, which for a large slit is equal to the width after appropriate normalization, this results in transmission steps directly proportional to the wavelength of the diffuse radiation [91M]. Another interesting analogy is to be found in the domain of quantum optics [99T] where the conductance of a beam of atoms, as defined by the ratio of the transmitted flux relative to the source brightness, can be shown to be quantized in units of $n\lambda_{dB}^2/\pi$, where λ_{dB} is the de-Broglie wavelength of the atoms in the incident beam. The observation of such a quantized atomic conductance requires a suitable confining waveguide and various microfabricated geometries have been suggested based upon the magnetic confinement resulting from the Zeeman potential.

3.3 Finite temperature

The effect of a finite temperature upon the conductance of ballistic QPCs is to introduce an energy scale $k_B T$ which leads to a thermal broadening of the device characteristics at elevated temperatures. At low temperatures the broadening between conductance plateaux is not limited by the ambient temperature but, in the context of the simple adiabatic model, by the geometry of the confining potential (see Section 3.1.4). Clearly, when the thermal energy becomes comparable with the subband energy spacing ($4k_B T \sim \Delta E_n$) the quantized structure will be significantly broadened.

For QPCs defined in heterostructure devices the subband energy spacing $\Delta E_n \sim \epsilon_F/n$ varies typically from $1-5$ meV as the channel width is changed. The typical temperature dependence of a high-quality QPC [91vW] is shown in Fig. 39 below.

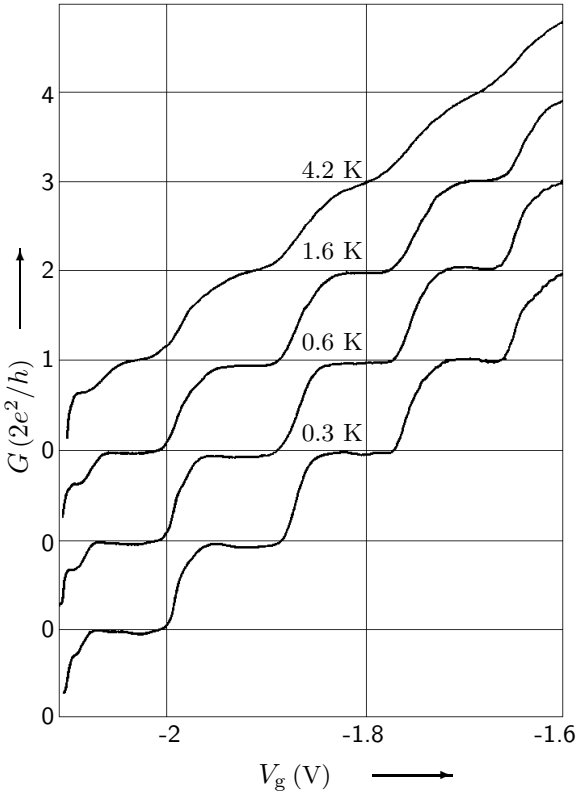

Fig. 39: The breakdown of the conductance quantization as a result of thermal averaging is illustrated. At elavated temperatures low-index plateaux disappear last due to the gate-voltage dependence of the subband energy spacing [91vW].

Larger subband energies have been attained in specially designed heterostructure devices [92S1] where the 2DEG is situated 30 nm from the Schottky gate electrodes used to define the QPC. Measurements of the gate-voltage characteristic and first derivative showed indications of quantized structure at temperatures up to about 40 K, and were in agreement with simple theoretical calculations of the conductance.

In a so-called "Butterfly-MOSFET" geometry [95T2], with a structured top gate used both as a diffusion mask and as an electrode to define a narrow inversion layer, measurements of the transconductance showed an anomolous peak close to threshold at temperatures up to 77 K which was attributed to ballistic transport. The lithographic width of the gate structure at its narrowest point was 0.24 μm, however the actual constriction width is estimated to be as small as 50 nm due to the effects of Born diffusion under the gate.

3.4 Sample geometry

As discussed in Section 3.1.5 above, the detailed shape of the confining potential can strongly influence the device conductance, especially when abrupt changes in the width or its first derivative with position occur. Whether such potential changes in real systems occur is however questionable. The majority of experiments have been performed in heterostructure devices where the conducting 2DEG lies typically $60-80$ nm beneath the surface. As such, the confining potentials induced via gate electrodes located at the surface are not expected to show abrupt potential variations as evidenced by the simulations of Fig. 29 [91N]. Indeed, the most rapid changes in channel potential are presumably more dependent on the local impurity potentials. This latter effect explains the mesoscopic character of QPC devices where nominally identical devices often show significantly different characteristics. The length resonances characteristic of WNW models have

been tentatively observed [91vW] in a finite number of samples, however the poor quantization in such devices suggests that the role of impurity scattering is equally important.

The dependence of the quantized conductance upon the channel length has been considered [89T] and it was shown empirically that the quantization breaks down for channel lengths considerably shorter than the elastic mean free path. For high-mobility heterostructures mean free paths of the order of 10 μm are typical, nevertheless ballistic QPCs much longer than 1 μm generally show poor quantization. The role of disorder has been considered above [91N] and agreement with the empirical data is found. Intuitively, the poor quantization can be understood as the ineffective screening of scattering potentials as the channel width narrows and the electron density decreases. Nevertheless, steps in the conductance have been observed for a long 10 μm, ballistic channel [96Y], defined using cleaved edge overgrowth. The values of quantized conductance were found however to deviate by as much as 25 % from the expected values. This experiment and other observations of quantized conductance in long 1D channels are considered more fully in Section 7.1.2(Part III).

The nature of the confining potential perpendicular to the current flow is of particular importance since it determines the subband spectrum of the QPC. Self-consistent solutions of related split-gate geometries in quasi-1D systems [86L, 88L1] suggest that at low densities the confining potential is almost parabolic. However, for higher electron densities the self-consistent solution of the Schrödinger and Poisson equations leads to the evolution of a truncated parabola, which is frequently modelled as a simple square well. A detailed analysis of the exact potential shape requires spectroscopic information about the subband energies as a function of gate voltage, and a particularly elegant method to determine the spectrum relies upon the magnetic depopulation of the 1D-subbands (as considered in Section 3.5). Both empirical data [89W2] as well as a simple theoretical model [89W1] have confirmed the validity of the above self-consistent analysis.

Experimentally, the most significant consequence of a realistic sample geometry is the collimation of the transmitted electrons (see Section 3.1.11) brought about by the adiabatic flaring of the QPC at its exit. Such an effect cannot be directly observed in the QPC resistance itself and was first investigated in a series configuration [88W2]. The observed gate characteristics suggest that the combined resistance is determined almost entirely by the narrower of the two QPCs. The

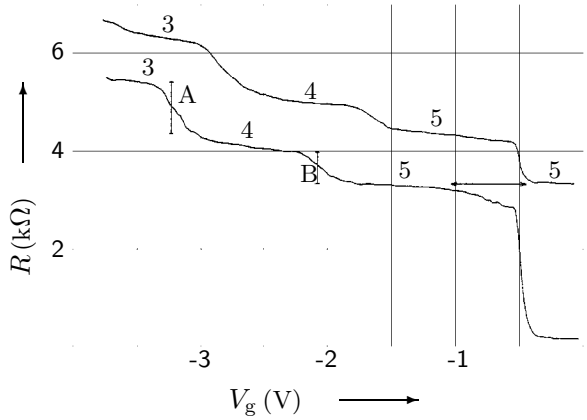

Fig. 40: The series resistance of two QPCs is plotted as a function of the gate-voltage applied to the first QPC device for two fixed values of the voltage applied to the second QPC device [88W2]. The steps in resistance indicated by the two vertical bars correspond to A = $h/24e^2$ and B = $h/40e^2$.

non-ohmic addition of resistance illustrated in Fig. 40 was initially interpreted as an indication of perfect transmission through both QPCs, however a more rigorous subsequent analysis [89B3] showed that the data could be best explained as the flaring of the QPC exit with a tapering collimation factor of roughly 2.5 as defined in Eqn. (55). Direct evidence for collimation has been found [90M2] in a series configuration where the injector and collector QPCs are separated by up to 4 μm. The transmitted electron beam can be shifted laterally by the application of a weak magnetic field and the angular distribution of the beam investigated. Typical results are shown in Fig. 41. From the height of the maximum at zero magnetic field a collimation factor of 1.85 has been determined and, under the assumption of adiabatic transport, was used to extract the angular distribution $P(\alpha)$ of the emerging electron beam $P(\alpha) = (f/2)\cos\alpha$ for $|\alpha| < \arcsin 1/f$.

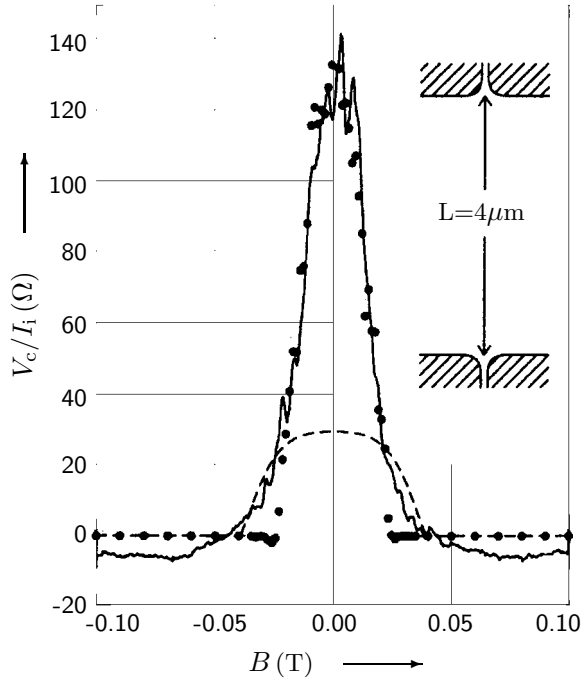

Fig. 41: The ratio of collector voltage to injector current is plotted as a function of the applied magnetic field for a QPC separation of $4\,\mu$m [90M2]. The dots indicate a simulation of the device configuration with tapering, and the dashed line the result of a simulation of an abrupt geometry.

The observed degree of collimation is tunable via the applied gate bias and scales linearly with the QPC resistance. Previous measurements of the collimation in a similar series configuration [89B4] however, were not able to find any significant variation of the collimation with channel width.

The angular distribution of the transmitted electrons in a single QPC [92O] has been carefully analysed as a function of the number of occupied subbands and typical data are shown in Fig. 42. The observed distributions are characteristic of diffraction at the QPC exit and have been successfully modelled [92S2] within a modified Fraunhofer diffraction theory (see also Fig. 33 above), which shows that the electrons propogate from injector to collector retaining both mode and phase information.

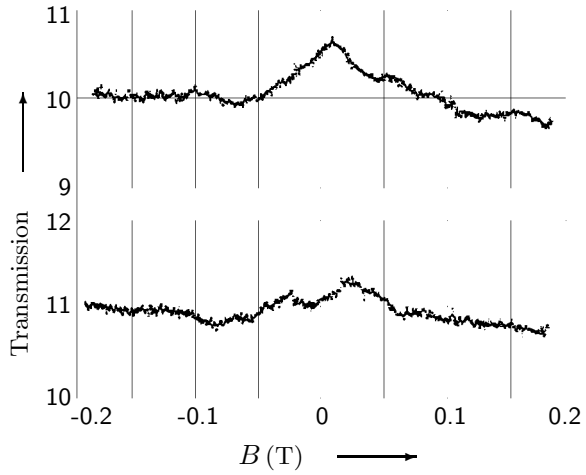

Fig. 42: The angular distribution of transmitted electrons (measured in arbitrary units of conductance) is measured via the application of a weak magnetic field [92O]. The upper and lower traces correspond to one and two occupied subbands respectively.

The interaction between parallel QPCs, defined using an air bridge technique to allow their simultaneous definition, was also investigated and the quantization in units of approximately $m\,n(2e^2/h)$ observed, where m is the number of parallel QPCs and n the number of occupied subbands [92O]. Similarly, measurements of the conductance in a parallel QPC geometry [89S4] have revealed quantization in units of $4e^2/h$ as illustrated in Fig. 43. In these experiments two nominally identical QPCs were defined using a single gate-electrode and an isolation resist tech-

nique to define the channels. The quality of the fabrication is evidenced by the almost perfect transitions between quantized values; close to pinch-off however indications of the emergence of structure at $h/2e^2$ and also at $h/6e^2$ suggest a small difference in lithographic width. Such par-

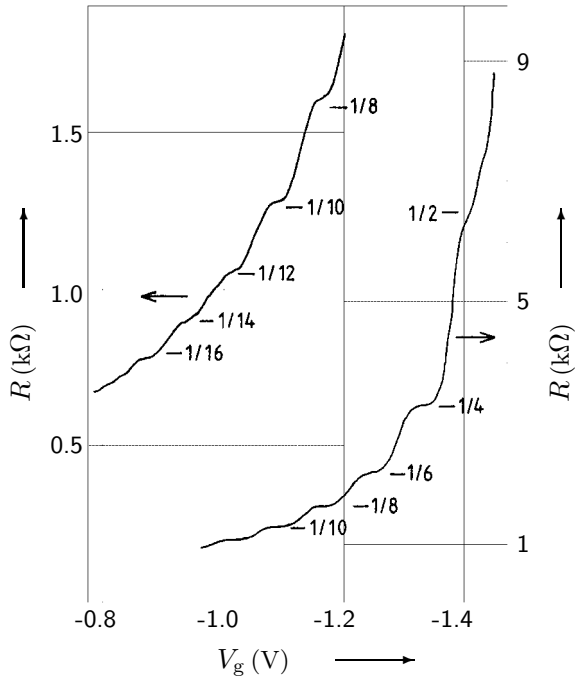

Fig. 43: The resistance of a parallel configuration of two ballistic QPCs is plotted as a function of the bias voltage used to define both channels simultaneously [89S4]. The fractions are marked in units of $h/2e^2$ showing that the conductance quantization occurs in units of $4e^2/h$.

allel configurations have been considered theoretically [93Y] and have been shown to have a rich conductance behaviour in a magnetic field, especially when the restriction of identical widths is relaxed.

The series configuration of QPCs also permits the measurement of a "Hall" voltage between the two QPCs. This possibility has been considered before to measure both the quenching of the Hall effect at small fields as well as the nature of the quantum Hall effect in the fractional regime. Simultaneous sweeps of both QPC gate electrodes have found an interesting correlation between the observation of quantized plateaux in the longitudinal resistance and mimina of the transverse resistance [91Y, 92Y3]. Such subband structure has been previously observed [91B2] although the quality of the sample was insufficient to ascertain the correlation with the conductance quantization. The interchange of the current and voltage contacts leads to qualitatively similar observations which go beyond the reciprocity relations associated with four-terminal measurements. It is argued that these observations are related to the existence of a cavity state between the two QPCs which couples weakly to the transverse contacts. However, in the context of the collimation effects discussed above, it seems more plausible that this effect is associated with a weakly asymmetric device configuration and the subband dependence of the focusing [92S2]. Indeed, subsequent experiments with samples of similar geometry [92Y1] have confirmed the original observation of conductance plateaux for series configurations and are consistent with the collimation picture detailed above.

The coupling between the subband states of a single QPC and those of an adjacent electron waveguide has been considered in a so-called T-geometry [94S, 95U], where electrons emitted from the QPC exit are injected into a narrow channel defined orthoganal to the emergent beam. The width of the electron waveguide is tuned via a reflector electrode, and both the waveguide conductance and QPC resistance simultaneously recorded (see Figs. 44 and 45). Oscillations in the QPC resistance are observed whose period is identical with that of the structure in the waveguide conductance, where conductance steps concordant with a change in the waveguide width of $\lambda_F/2$ are seen. This effect has been interpreted in terms of the mode coupling between the waveguide states and the emergent electron beam. A detailed numerical analysis of this effect [95U] has been

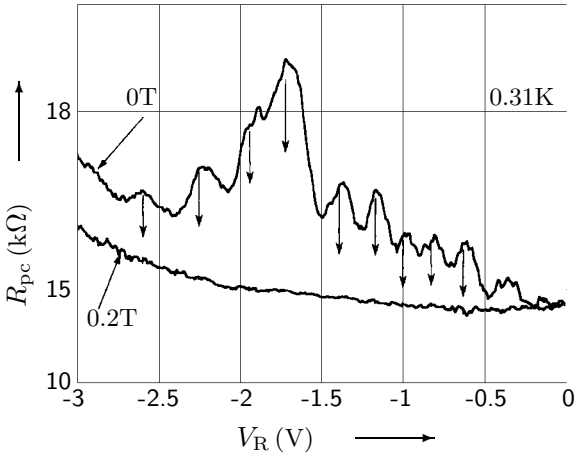

Fig. 44: The QPC resistance is plotted as a function of the reflector-gate bias for magnetic fields of 0 T and 0.2 T at a bath temperature of 0.31 K and for fixed QPC-electrode bias of -2.9 V [95U]. The arrows indicate structure correlated with the waveguide conductance as shown in Fig. 45.

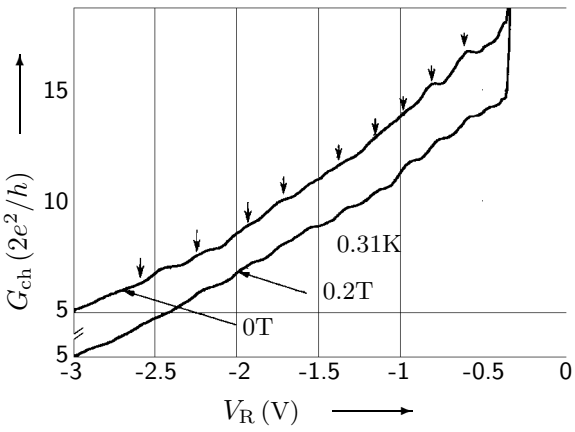

Fig. 45: The conductance of the waveguide is plotted as a function of the reflector-gate bias with identical experimental conditions as in Fig. 44 [95U]. The arrows indicate the correlated structure between the channel conductance and QPC resistance of Fig. 44.

able to reproduce the important features of the experiment, and also shows that the suppression of the effect at finite magnetic fields is associated with the formation of edge states within the waveguide channel. An important feature of this model is the requirement of a rounded geometry at the interface between QPC and waveguide, without which the magnetic field data cannot be simulated.

The wave nature of the transmitted electronic states has also been considered in geometries where the QPC is situated in a resonant cavity [89S3, 97K1]. In the original experiment [89S3] the transmission through the QPC was modulated by shifting the potential induced by a reflector gate. The resulting oscillations had a period given by $\lambda_F/2$ as expected. The resonance condition $n\lambda = 2L$, where L is the separation between reflectors, must be modified due to an additional phase shift arising from a change of the wavevector within the QPC, an effect which is most clearly visible when the number of occupied subbands is small. More recently a similar geometry with cirular reflectors [97K1] has been used to investigate coherent resonant tunneling in the conductance of the QPC device. Similar periodic data were obtained and modelled using a so-called wavelet boundary wall method. The model predicts periodic conductance peaks and additional fine structure due to stable modes within the approximately circular cavity.

3.5 Magnetic field

In the presence of a perpendicular magnetic field the purely electrical quantization within the channel is modified, and hybrid magneto-electric subbands evolve. For the conductance of a QPC device this results in a reduction of the number of subbands within the channel for a given channel width, and hence to the observation of magnetic depopulation of subbands as the magnetic field strength is increased. The original observation of this effect in QPCs [88W1] is shown in Fig. 46, where it is seen that the number of plateaux observed within a given voltage range decreases with increasing field. Furthermore, the plateaux are more pronounced and, in a two-terminal measurement setup, the quantized values of conductance are maintained.

The first attempt to model the magnetic depopulation in QPCs [88vW2] assumed a square well confining potential and calculated the number of occupied subbands as a function of the channel width and magnetic field strength according to a simple semi-classical quantization rule, which

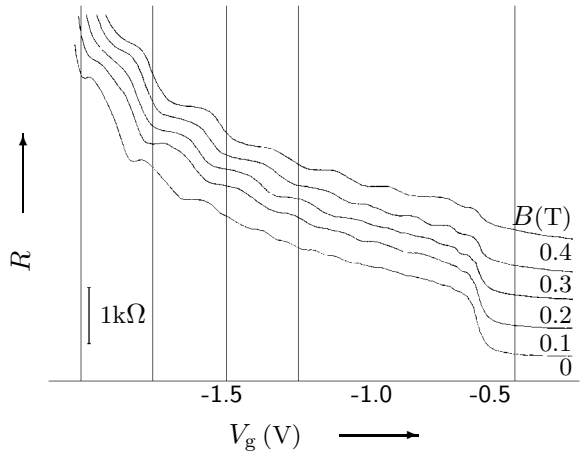

Fig. 46: The QPC resistance is plotted as a function of gate bias at weak perpendicular magnetic fields from 0 to 0.4 T. The measurements were taken at $T = 0.3\,\mathrm{K}$ and the curves are offset vertically by $500\,\Omega$ for clarity [88W1].

yields

$$n(B) = \mathrm{Int}\left\{\frac{k_\mathrm{F} l_\mathrm{c}}{\pi}\left[\arcsin\frac{W}{2l_\mathrm{c}} + \frac{W}{2l_\mathrm{c}}\sqrt{1-\left(\frac{W}{2l_\mathrm{c}}\right)^2}\right]\right\} \tag{60}$$

where l_c is the cyclotron radius. The resulting $n(B)$ can be directly compared with the number of occupied subbands from the conductance data (see Fig. 47) for a given gate voltage (and hence channel width). The resultant fit is illustrated in Fig. 48 and permits the gate voltage dependence of the channel width and 2D-carrier density to be extracted; for the gate-voltages considered an essentially linear variation for both parameters is found. Furthermore, a good fit to the data could only be obtained by assuming the existence of an additional potential barrier at the entrance to the QPC, whose height increased with the applied negative bias.

A more detailed analysis [89W2] based upon a realistic confining potential in the absence of disorder, as discussed above in Section 3.4, relies upon a variational calculation of the spectrum of the subband energies within the QPC channel at a given field strength and channel width. As above, the conductance data at fixed V_g are compared with the predictions of the calculation and hence the system parameters determined. An almost linear variation of channel width and 1D-density are found, and the extracted Fermi energy shows little change with respect to the bulk value. This suggests that the energy barrier at the entrance and exit of the QPCs becomes important only shortly before pinch-off when the self-consistent potential screening becomes weaker. The quantitative features of the above model have been reproduced in a simpler analytical description of a QPC based upon parabolic confinement [89W1], which also yielded qualitative agreement with the semi-classical model.

At higher magnetic fields the lifting of the spin-degeneracy gives rise to additional quantized plateaux at values of $(2n+1)\cdot e^2/h$ independent of the orientation of the magnetic field [88W1, 88vW2]. Furthermore, the electronic transport occurs in edges channels located at the sample boundary. When such edge states propogate through ballistic QPCs the width of the QPC channel modifies the transmission of the uppermost states [89vW2, 91vW], and thus enables the selective population and detection of these edge states. In the quantum Hall regime the selective population of edge states leads to the observation of anomolous integer plateaux [89vW2] where the channel conductance remains quantized independent of the number of occupied Landau levels in the bulk of the sample (see Fig. 49). Using the Landauer-Büttiker formulation for transmission in multiprobe geometries, the conductances between a bulk 2DEG and two closely situated QPCs have been calculated. In the absence of scattering, the first QPC can be employed to selectively populate edge states which can then be selectively detected at the second QPC. This configuration of QPCs plays an important role in many subsequent experiments [94W, 99H] where scattering between the selectively occupied and unoccupied subbands in the 2D bulk between QPCs can be investigated.

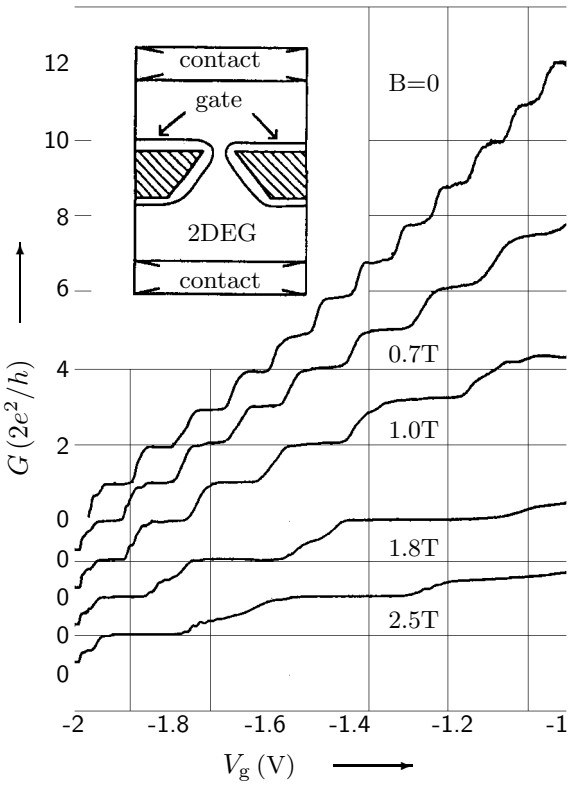

Fig. 47: The QPC conductance is shown as a function of the gate bias for several values of magnetic field and at a temperature of 0.6 K [88vW2].

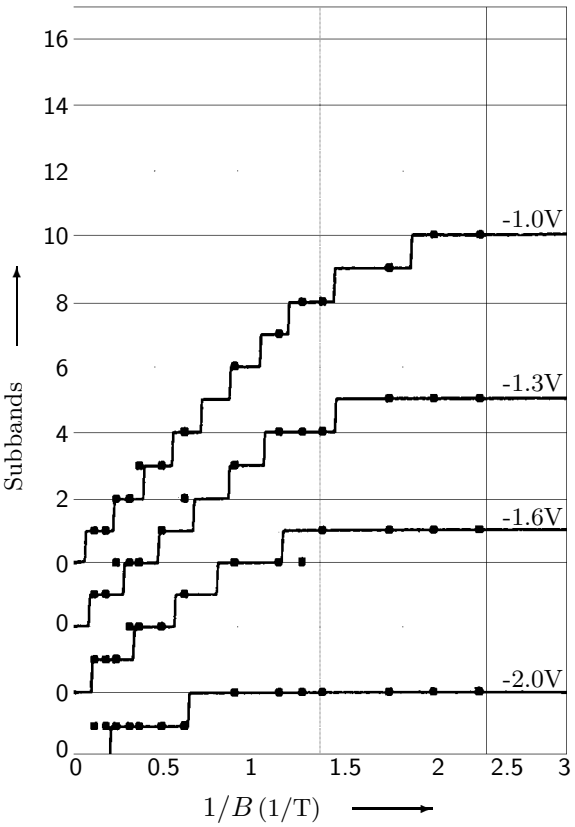

Fig. 48: The number of spin-degenerate subbands are shown (square dots) as a function of the inverse magnetic field strength for several vlaues of gate bias [88vW2]. Full lines represent the model fit.

An early example of such scattering effects is the suppression of the SdH-oscillations observed when either the injected current does not populate the uppermost Landau level, or the detection of the uppermost Landau level is selectively suppressed. This effect is illustrated in Fig. 50 and has been employed to extract interedge scattering rates within the 2D bulk. At high magnetic fields it has been shown that ballistic transport can occur on macroscopic length scales in excess of several hundred microns [89vW3].

Oscillatory behaviour in the presence of a perpendicular magnetic field has been observed in QPC devices [88vL, 89W3] and has been attributed to the AB-effect in singly connected geometries. In the data of Fig. 51 clear periodic oscillations are seen with periods varying from $\Delta B = 0.056\,\mathrm{T}$ to 0.18 T corresponding to areas of $(250\,\mathrm{nm})^2$ and $(150\,\mathrm{nm})^2$ respectively. The existence of a well-defined area within a singly connected QPC geometry is somewhat suprising, and together with the observation that such structure is not common in QPC devices, suggests that some backscattering mechanism in the vicinity of the QPC is operative. Comparable data are presented in Fig. 52 and a weak (25 %) gate voltage dependence is observed suggesting that the periodic oscillations are associated with a change in the channel geometry. In both instances the areas required are comparable with the inner area, as defined in a WNW picture, although no clearcut barriers for reflection are defined. For the controllable observation of AB-oscillations, structures with well-defined barriers integrated into the defining geometry [89vW1] should be considered.

The transverse electron focusing of ballistic electrons in the presence of a perpendicular magnetic field [88vH, 89vH] has been reported in QPC devices. Such experiments can be exploited to investigate the nature of the scattering processes in metallic systems. Typical data are shown

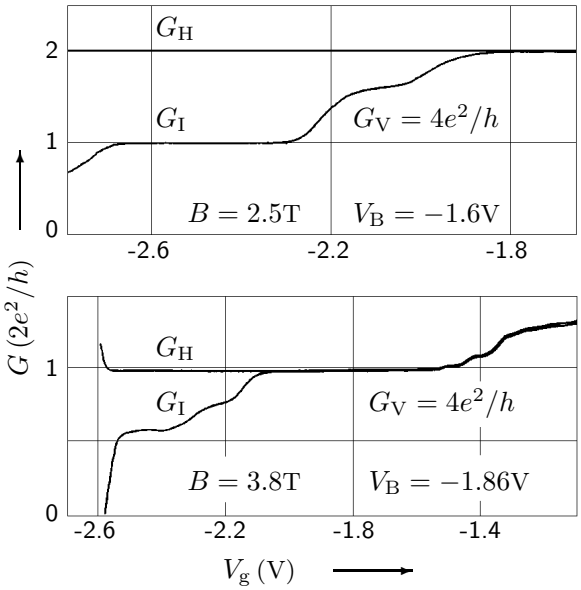

Fig. 49: A comparison between the two-terminal conductance G_I and the Hall conductance G_H is illustrated for two different values of the two-terminal conductance of the voltage probe G_V. The important point is that G_H follows the maximum of the conductances (G_V, G_I) and remains quantized whenever either of these values is quantized [89vW2].

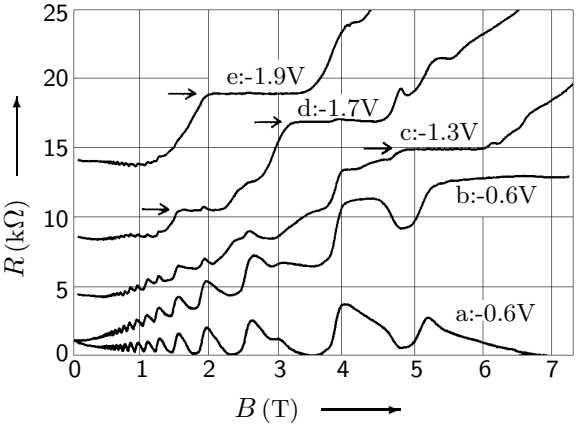

Fig. 50: The resistance of a 2DEG is plotted as a function of the prependicular magnetic field for four different QPC gate voltages. The suppression of the SdH oscillations resulting from the selective detection of the edge states is clearly illustrated [89vW3]. For trace a) the direction of the magnetic field has been reversed.

in Figs. 53 and 54 where the collector voltage is plotted as a function of the applied magnetic field. In these experiments electrons are injected into the bulk 2DEG material via a QPC and are focused under the influence of the magnetic field into a collecter QPC. The voltage build-up in the reservoir behind this collector is a measure of the efficiency of the focusing. At low magnetic fields the observation of multiple peaks shows that the ballistic trajectories scatter specularly on the boundary potential defined by the gate electrode of length L separating the two QPCs. The additional reproducible fine structure seen at low temperatures is smeared out by an increase in the applied bias, or equally through a widening of the injector QPC, as shown in Fig. 54. In order to explain the fine structure seen in these experiments the propogation of the injected electrons in magnetic edge states must be accounted for. At low temperatures the interference of these states leads to the observed fine structure when phase coherence is maintained.

Increasing the injector bias leads to the observation of a shift in the peak positions related to the classical focusing orbits [90W3] as is shown in Fig. 55. This effect can be explained in terms of the additional kinetic energy that the injected electrons have in the bulk 2DEG. Using a simple phenomenological model for the voltage drop over the injector QPC, it has been shown that the gain in kinetic energy is linear over a wide range of applied bias, and that the voltage dropped over the QPC is in good agreement with the quantized value. Furthermore, the observation of focusing suggests that ballistic transport occurs for significant lengths despite the excess kinetic energy (up to 50 % of E_F). Comparable experiments have also been performed in a series geometry [89S2] where electrons emitted through an injector QPC are collected via a tunable collector QPC 2 μm away. The transfer ratio, i.e. the effeciency with which emitted electrons reach the collector, has been measured as a function of the injection energy, and it has been found that the dominant scattering mechanism is the emission of LO-phonons. Below the LO-phonon energy scattering is weak and ballistic lengths comparable to those discussed above are found. Similar experiments

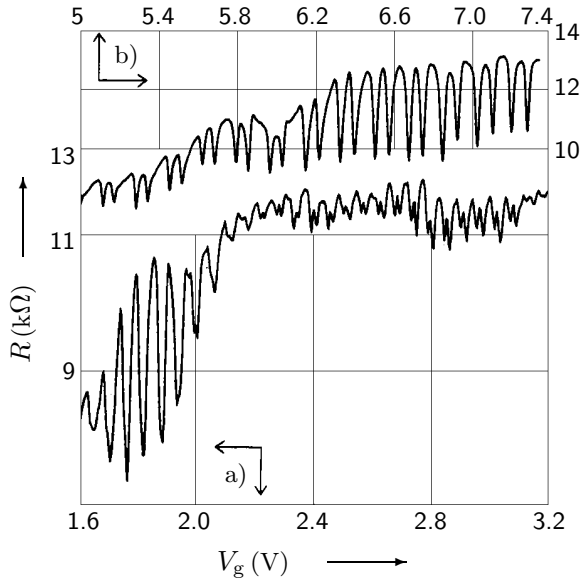

Fig. 51: The QPC resistance at a fixed gate voltage of $V_g = -1.7\,V$ is plotted as a function of magnetic field for two different field regions corresponding to a) the transitions between the $n = 4$ and $n = 2$ spin degenerate hybrid subbands and b) between $n = 2$ and $n = 1$ at fields sufficient to lift the spin degeneracy [88vL].

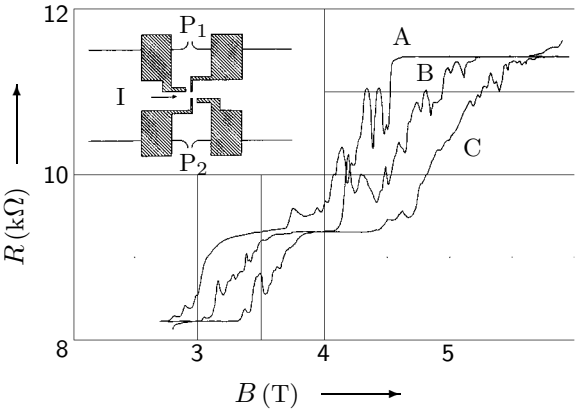

Fig. 52: The magnetoresistance of the QPC device, shown schematically in the inset, is plotted for three different gate voltages for the transitions between $n = 4, n = 3$ and $n = 2$. The measurment geometry permits the quasi-two-terminal device conductance to be determined, which clearly shows the excellent device quantization [89W3].

have been perfrormed in an electron optical setup where the collection efficiency is improved via the application of an electrostatic gate electrode operating as an electron lens [92S3].

In the focusing experiments above, the injector and collector reservoirs are electrically separated from each other by the gate electrode which also acts as a specular reflector for the focusing experiments. In a parallel configuration of QPCs [95E] electron focusing has been inferred from measurements of the magnetoresistance at low fields. The classical focusing of the transmitted electrons leads to an effective reflection and hence to peaks in the resistance.

3.6 Impurities

Impurity scattering ideally plays a subsidiary role in determining the device characteristics of a perfect QPC. Nevertheless, in real devices the effects of impurities cannot be ignored, and the characteristics of nominally identical devices are frequently significantly different. A variety of phenomena associated with impurities are reflected in the dynamic properties and are considered more fully in Sections 4.1.5 and 4.6. An early observation of resonant structure in the gate characteristic close to pinch-off [90M1] has been attributed to the tunneling through an isolated impurity (see Fig. 56). In this instance the QPC characteristics permit the spectroscopy of the impurity state, which has been investigated as a function of temperature and magnetic field. Similar effects close to the pinch-off region have been subsequently observed in Si/SiGe QPCs [95T4] and have been analyzed using the same theoretical framework [88K3].

A particularly elegant method exploited to investigate the nature of the confining potential, or rather its modification due to impurities, relies upon the lateral shifting of the channel position when different voltages are applied to the split-gate electrodes [90W2]. In such experiments the resistance associated with a given number of conducting subbands shifts with the applied differential voltage, and reflects the change in transmission resulting from changes in the local potential

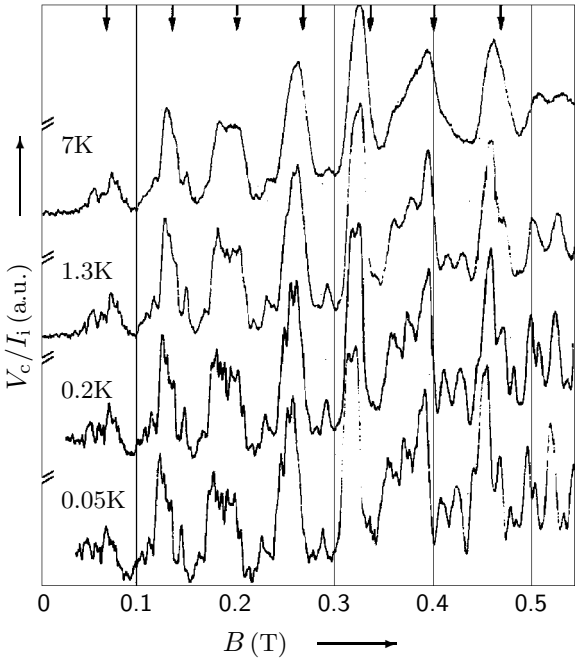

Fig. 53: Typical electron focusing spectra are plotted as a function of the applied field for temperatures between 7 K and 50 mK. The peak positions predicted by $B_{\mathrm{focus}} = 2i\hbar k_{\mathrm{F}}/eL$ are indicated by the arrows ($i = 1, 2, 3, \ldots$) [89vH].

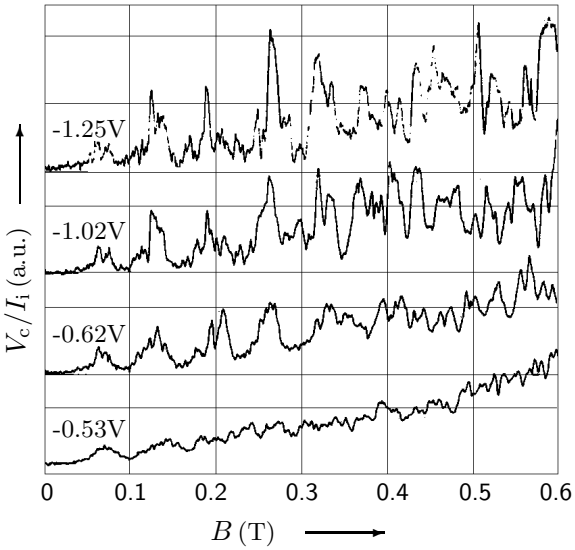

Fig. 54: The gate-voltage dependence of the electron focusing spectra are shown for a bath temperature of 50 mK. The number of occupied channels decreases with increasing negative gate bias [89vH].

landscape. In one device the suppression of plateaux (see Fig. 57) has been interpreted as a measurement of the coupling of the transverse wavefunctions with the reservoirs which, due to the presence of a strongly localized impurity, are modulated with channel shifts of the order of $\lambda_{\mathrm{F}}/4$. The lateral shifting technique has been considered theoretically [94L1] and a device proposed consisting of four electrodes; two shift the saddle point of the QPC constriction laterally, and two additional gates located towards source and drain reservoirs shift the position of the saddle point along the channel. It it suggested, that in such a device it is possible to extract the correlation length of the impurity potential, an important parameter for the realistic modelling of the impurity potential.

The influence of DX centres, located within the doped layer of the heterostructure, on the QPC characteristics has been investigated [98H] as a function of temperature and also after irradiation with light. Although the temperature dependence of the carrier concentration of the 2DEG is relatively weak, the pinch-off voltage of the QPC moves to significantly lower negative voltages as the carriers within the doped layer freeze out. Irradiation has the effect of increasing the carrier density within the dopant layer, and hence leads to the observation of more negative pinch-off voltages for the QPC. Indeed, the screening of the gate potential can be so effective that no constriction is formed in the 2DEG.

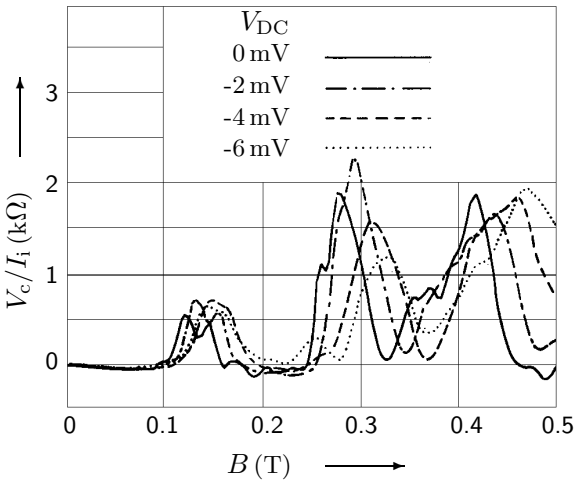

Fig. 55: The electron focusing peaks at low magnetic field are shown for different applied injector bias [90W3].

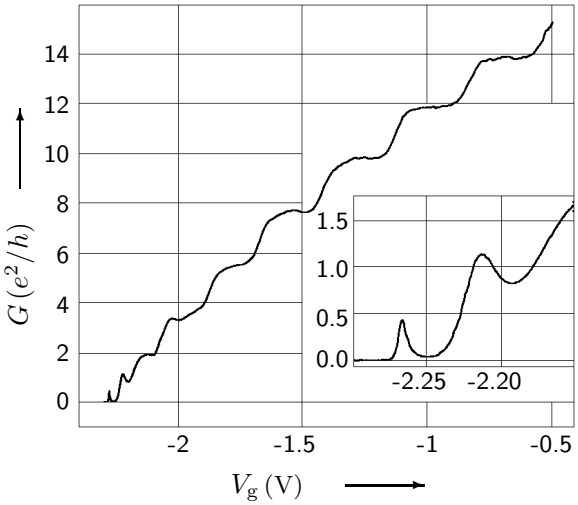

Fig. 56: The conductance of a ballistic QPC is plotted as a function of the applied gate bias for a bath temperature of 550 mK. The inset shows the resonant structure close to pinch-off [90M1].

3.7 Interactions

Electron-electron scattering is an important phase-breaking mechanism in semiconductor heterostructures at low temperatures. A convenient method to study this mechanism is based upon the collimation geometry discussed in Section 3.4. The influence of changes in the scattering rate, induced here by changes of the experimental conditions, is monitored by the detected collimated beam [92M1]. The important experimental result is shown in Figs. 58 and 59, where the collimation signal is plotted as a function of the magnetic field. The influence of a DC current flowing at right angles to the ballistic, injected current is seen to be similar to the influence of an elevated temperature. As discussed below (see Section 3.11) the local electron temperature can be derived from experiments of the thermopower in a QPC device. This technique has been used in these collimation experiments to show that the reduction of the collimated signal is related to the increase in electron temperature and not directly to the absolute lattice temperature. It is thus concluded that the relevant scattering mechanism for the ballistic electron beam at the injection energies considered is electron-electron scattering, in good agreement with theoretical models for 2DEG systems. Similar conclusions [95M3] have been reached in an electron focusing geometry at injection energies up to 15 meV (cf. 36 meV for the LO-phonon energy).

As considered in Section 3.1.6 above, at filling factor $\nu = 1/2$ the properties of a 2DEG are expected to be given by the behaviour of so-called composite fermions. The ballistic resistance in QPC devices at this filling factor has been measured [96L1, 96L2] and despite an elastic mean

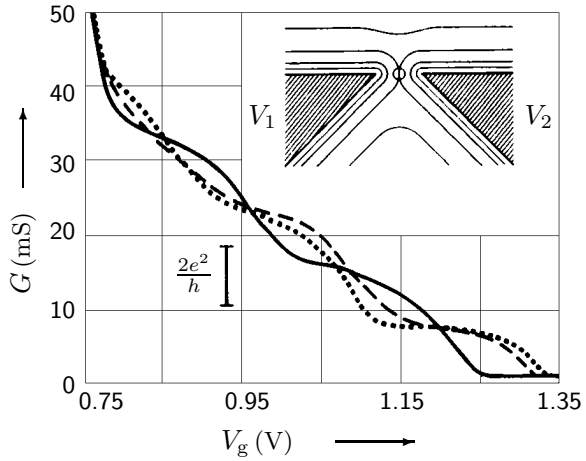

Fig. 57: The conductance of a QPC device is plotted as a function of the average gate bias for three values of differential bias. Two traces show clear quantization for even plateaux ($\Delta V_g = V_1 - V_2 = +0.30\,V$ and -0.42 V) whilst the trace for $\Delta V_g = -0.06\,V$ shows the odd plateau [90W2].

free path for the composite particels of 0.7 μm, longer than the QPC channel, no evidence for conductance quantization could be found. The gate characteristic showed a monotonic increase of resistance with applied gate voltage, albeit with significantly higher values of resistance for the composite fermion state. The width of the channel was determined for both instances and showed a linear dependence with the applied gate bias but with narrower channels for the $B_{\text{eff}} = 0$ case, in agreement with theoretical models where the confining potentials of composite fermions are sensitive to variations in the local electron density.

3.8 Electron spin

The conductance quantization in units of $2e^2/h$ reflects the spin degeneracy of the electronic states within the QPC, and therefore differs from the fundamental unit of conductance observed in the quantum Hall regime. A lifting of this spin degeneracy gives rise to additional conductance plateaux at $(n + 1/2) \cdot 2e^2/h$ as discussed in Section 3.5 and offers, at least in principle, a method for determining the intersubband energy spacing of the 1D electronic states within the QPC. In practice the magnetic field strengths required to lift the spin-degeneracy, with the field applied in a parallel orientation, are considerably larger than expected and suggest that the effective g-factor is significantly enhanced compared with the bulk value of GaAs. As discussed in Section 3.1.6 in the adiabatic approximation the observation of a spin-splitting should only be observed for high index plateaux with

$$n > n_c = \left(\frac{2}{\pi}\right)^2 \frac{\lambda_F}{R} \left(\frac{E_F}{g\mu_B B}\right)^2 \tag{61}$$

as seen in experiment and illustrated in Fig. 60. For the QPC under consideration an estimate of the radius of curvature of the confining potential at definition then permits an estimation of the maximal effective g-factor of about 0.86 (cf. 0.44 for bulk GaAs).

A fascinating application of the lifting of the spin degeneracy in QPCs is to be found in their use to locally create and probe the dynamic nuclear polarization in a AlGaAs/GaAs heterostructure [94W]. The nuclear and electronic spins interact via the hyperfine interaction, in which the change of an electron spin is accompanied by an associated change of nuclear spin. This effect can either be used to create a net nuclear polarization, or the dynamic nuclear polarization can be used to change the transport properties of spin polarized electrons. In this context the ability of a QPC to selectively transmit and reflect the edge states created in a perpendicular magnetic field can be usefully exploited (see Section 3.5). The geometry chosen for the experiments is essentially that of an isolated 2DEG connected to reservoirs via QPCs at entrance and exit (see Fig. 61). The perpendicular magnetic field strength is set to give a bulk filling factor $\nu = 2$ while the QPCs are tuned to transmit only the lower edge channel with spin-up oriented electrons. In the isolated 2DEG region interedge channel scattering can occur which results in a reduction of the current

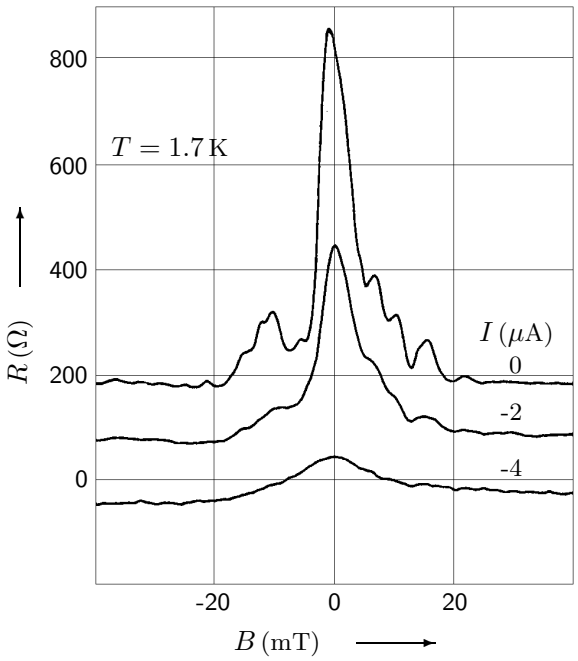

Fig. 58: The collimation resistance is plotted as a function of magnetic field for various current strengths flowing in the ballistic region between QPC injector and collector [92M1]. For clarity the curves are offset vertically.

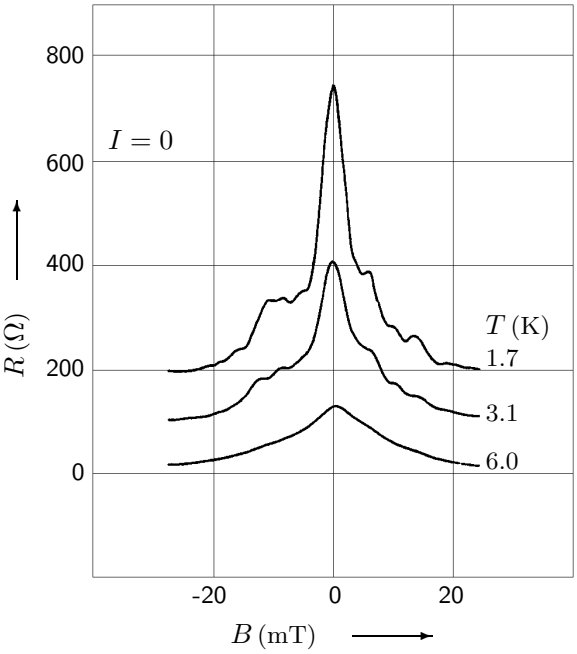

Fig. 59: The comparable measurement (see Fig. 58) of the collimation resistance is shown for various device temperatures [92M1].

transmitted through the detector QPC. Although a number of mechanisms can contribute to the interedge scattering the nuclear spin scattering process clearly manifests itself in a pronounced hysteresis at large applied bias, as illustrated in Fig. 62. The nuclear origin of this signal was confirmed by fixing the applied bias to the hysteretic region and applying an rf-signal to the gate electrode of the detector QPC. The resonant structure observed could be clearly correlated with NMR signals associated with the As and Ga nuclei.

In very clean 2DEG systems the conductance characteristics of some QPCs have shown an additional conductance feature beyond the last conductance plateau [96T3]. It has been suggested that this feature is an intrinsic property of very clean 1D channels; furthermore the clear evolution of the spin-split conductance plateau in a large parallel magnetic field (see Fig. 63) from this anomolous feature have led to the suggestion that the 1D gas is spin-polarized in zero magnetic field.

3.9 Statistical properties

Ever since the original observation of photon bunching in the correlated intensities of two coherent light beams [56HB] the observation of a statistical correlation in a fermionic system has remained an elusive goal. Despite vast improvements in the coherence of electron sources the measurement of anti-bunching has yet to be conclusively demonstrated in free electron systems. It may therefore seem somewhat suprising that experiments on QPC devices have indeed shown such second-order coherence effects, but in fact the high degree of phase space occupation makes the observation of electron anti-bunching in the solid state readily possible [98L, 99H].

The first experiment to demonstrate anti-bunching in the solid state was based upon the interaction between two ballistic beams which are partially transmitted through a mesoscopic beam splitter [98L]. In this experiment the QPCs are used to produce the two collimated beams of

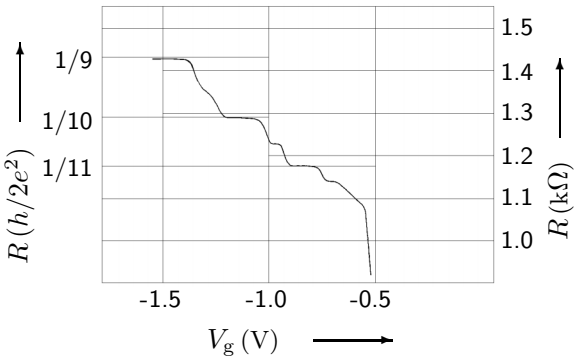

Fig. 60: The channel resistance of a typical QPC device is plotted as a function of the applied gate-voltage in the presence of a large parallel magnetic field, $B = 13.6$ T at $T = 100$ mK. The spin-splitting gives rise to additional quantized plateaux at $R = h/23e^2, h/21e^2$ and an incipient plateau at $h/19e^2$ [88W1].

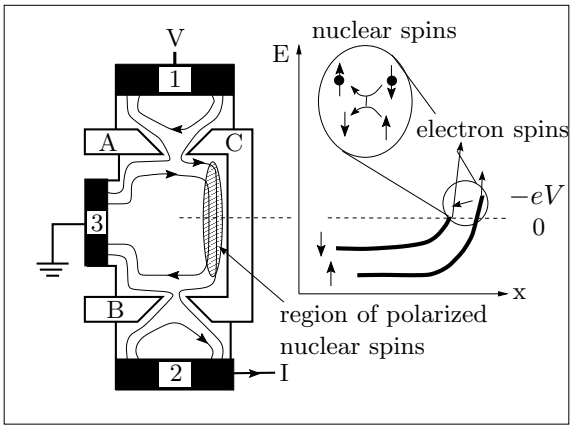

Fig. 61: A schematic illustration of the geometry employed to investigate the electron-nuclear spin interaction [94W]. Ohmic contacts are shown as dark regions, and the gate eletcrodes A,B and C are also shown. The energy level diagram associated with the edge states occupied within the central region of the device is plotted and the possible scattering mechanism in this region is illustrated.

ballistic electrons with zero current noise as discussed in Section 4.6. With the transmission of the QPC adjusted such that the conductance is exactly $2e^2/h$ the partition noise of the current through the QPC is completely suppressed. In a configuration such that the two ballistic beams interact in the vicinity of the beam splitter the current noise of one of the two output beams can be directly compared with that measured in the output beam when the two QPCs are separately biased (see Fig. 64). The observed suppression of the output current noise is a clear manifestation of fermionic anti-bunching and can be well explained within the context of the model parameters assumed in the experiment.

An alternative approach to investigate the fermionic correlations of electrons has been realised in transmission experiments through a QPC in the quantum Hall regime [99H]. The transmission and reflection of the current carrying edge states clearly manifests the anti-bunching of electrons, as seen in the autocorrelation of the transmitted current and the cross-correlation of the transmitted and reflected channels (see Fig. 65). These current fluctuations normalised to unit frequency bandwidth are expected to yield

$$\langle \Delta I_\alpha \Delta I_\beta \rangle_s = \pm 2e|I|t(1-t) \tag{62}$$

where t is the transmission of the edge state through the QPC. For the experimental situation with $t = 1/2$ excellent agreement with the observed current correlations is found.

3.10 Non-linear effects

The first experimental investigation of the non-linear properties of ballistic QPCs [89K6] manifested large nonlinearities in the current-voltage characteristics for applied biases comparable with the subband energy spacing. As discussed in Section 3.1.10 above the differential conductance is expected to show additional plateaux structure as the quasi-Fermi energies of source and drain

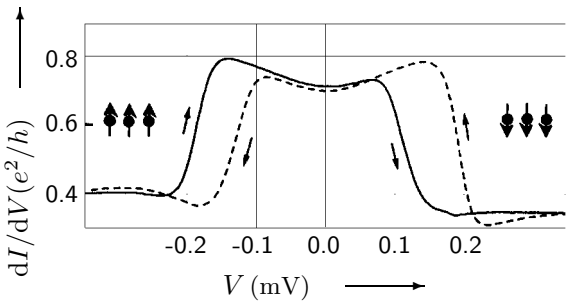

Fig. 62: The differential conductance dI/dV is plotted against voltage V at $T = 50\,\mathrm{mK}$ and $B = 4\,\mathrm{T}$ ($\nu = 2$). The solid lines indicate upward and the dashed lines downward voltage sweeps [94W].

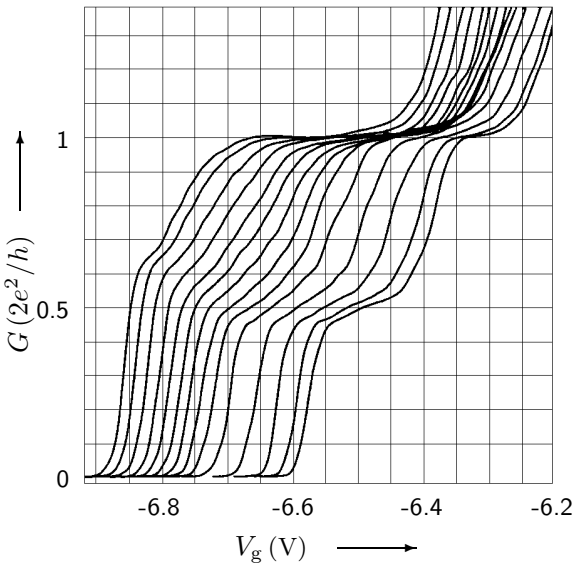

Fig. 63: The first conductance step showing the emergence of the spin-split conductance step at e^2/h from the anomolous conductance feature at $0.7(2e^2/h)$ as the parallel magnetic field is increased from 0 T to 13 T (the curves are offset for clarity) [96T3].

reservoirs shift relative to the subband energies. This behaviour is also reflected in the change of slope of the observed current-voltage curves. Under the assumption of an approximately symmetrical voltage drop along the QPC the data were used to extract a breakdown voltage V_{BR} whose maximal value yields the intersubband energy as illustrated in Figs. 66 and 67. The empirical value for the intersubband spacing was found to be in good agreement with the corresponding value extracted from magnetic depopulation data (see Section 3.5).

An interesting extension of the above discussion considers the effect of a magnetic field upon the non-linear characteristics in an asymmetric geometry [92N2]. When the voltage drop along the channel length is not symmetric then the differential conductance of the QPC is expected to show conductance values of $(n+\beta)\cdot 2e^2/h$ and $(n+\beta-1)\cdot 2e^2/h$, where n is number of conducting one-dimensional subbands in the linear regime and β the fraction of the voltage dropped at the entrance to the QPC. Which of the above conductance values is observed depends upon the energy separation between chemical potential and the respective subband minima. By considering the difference between the non-linear characteristics observed for positive and negative applied bias and, assuming that the fraction β depends solely upon the device geometry, the value for β has been extracted. In zero magnetic field there is no significant difference between the two polarities, $\beta = 1/2$, and the potential drop is essentially symmetric despite the intentional asymmetry of the QPC geometry itself. In the presence of a perpendicular magnetic field the non-linear characteristics show a significant difference between the two polarities which saturates for high applied bias according to $\Delta I = (2\beta - 1)V \cdot 2e^2/h$. The value of β thus obtained was roughly 0.6 independent of the applied gate bias and has been attributed to the asymmetry of the current flow along the edges of the QPC geometry in the presence of a perpendicular magnetic field.

A more systematic investigation of the non-linear properties over a wider range of gate-voltages

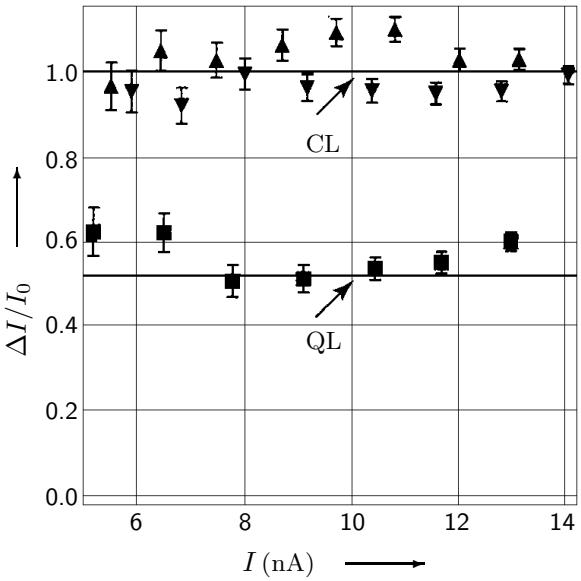

Fig. 64: The suppression of collision noise in an electron beam splitter is illustrated as a function of the output current. The quantum mechanical result (QL, two-fermion collision noise) after normalization and correction for zero bias offset shows a significant reduction when compared with the classical result (CL, single-particle partition noise) [98L].

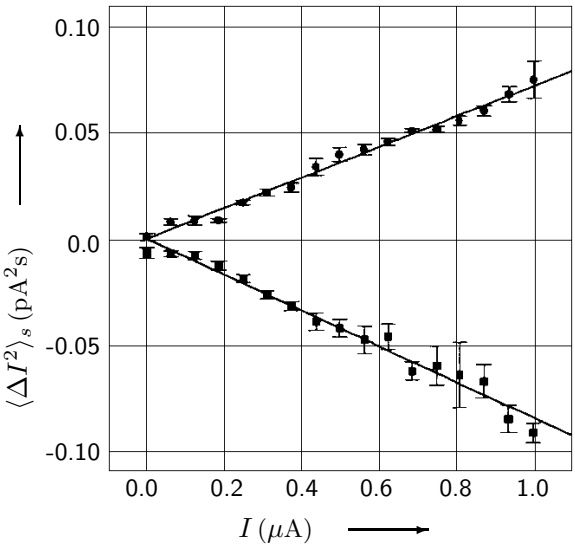

Fig. 65: The measured auto-correlation of the transmitted current and cross-correlation between transmitted and reflected currents are shown as a function of the total current through the QPC device. The experimental values of the slopes are $+0.23 \cdot 2eI$ and $-0.26 \cdot 2eI$ in excellent agreement with the experimental transmission [99H].

where several subbands within the QPC are occupied has also been considered [90P, 91P1, 92P2, 91P2]. The prediction of the evolution of half-integer plateaux [88G1, 89G1] with conductance values $(n + 1/2) \cdot 2e^2/h$ has been confirmed as illustrated in Fig. 68. In particular the variation of the subband energy separation with subband index can be investigated and it was suggested that a parabolic confining potential was best suited to explain the observed data, where no significant increase of subband spacing with index was found.

The influence of a magnetic field upon the additional quantized plateaux is illustrated in Figs. 69 and 70 [91P1, 91P2]. In the absence of a magnetic field the additional half-integer plateaux are observed as before; furthermore additional anomolous structure is observed at values of roughly $0.85 \cdot 2e^2/h$ and at $0.2 \cdot 2e^2/h$ which cannot be explained within the theoretical model discussed above [88G1, 89G1]. With a perpendicular magnetic field applied all quantized structure becomes more pronounced as a consequence of the increased adiabaticity through the QPC. Not only are the half-integer plateaux clearly visible but, in addition, the reemergence of the original integer quantization can be discerned at $4e^2/h$. The anomolous structure previously observed at $0.85 \cdot 2e^2/h$ has disappeared. In the presence of a large parallel magnetic field the Zeeman spin-splitting is sufficient to lift the degeneracy of the spin states (see Section 3.5 above) and the same behaviour can now be observed for quantized states $G = ne^2/h$ in the linear response limit which split into quantized states $(n + 1/2) \cdot e^2/h$ at high bias [92P2].

For higher applied bias ($eV_{\rm sd} \gg \Delta E$) the current-voltage characteristics of some QPCs have been found to show pronounced instabilities [89B5] and it has been suggested that these are related to the formation of current filaments within the one-dimensional channel, although these reports remain unconfirmed, as does the observation of Coulomb-staircase like behaviour in a single QPC [90B1].

The non-linear properties of QPCs have also been investigated in the tunneling regime where their characteristics have been exploited to characterize the potential along the channel length

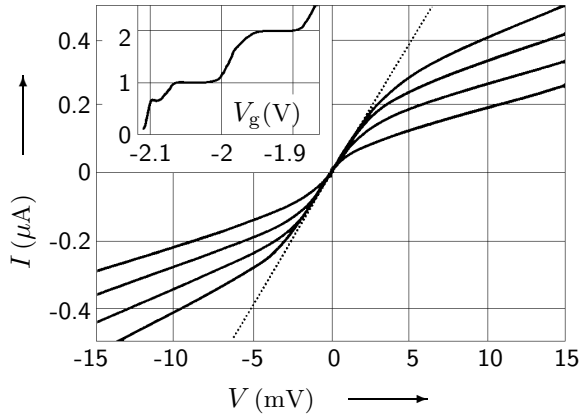

Fig. 66: The current-voltage characteristics of a ballistic QPC in the non-linear regime for gate voltages (V_g) between -2.0 V and -2.05 V. Here only one subband is occupied and the small-signal conductance is, as expected, $2e^2/h$ as shown in the inset [89K6].

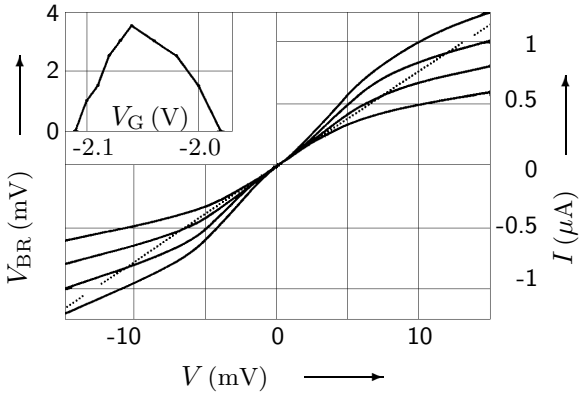

Fig. 67: The current-voltage characteristics of a ballistic QPC in the non-linear regime for gate voltages (V_g) between -2.05 V and -2.1 V. The inset shows the breakdown voltage, where a 1 % deviation from quantized conductance is observed [89K6].

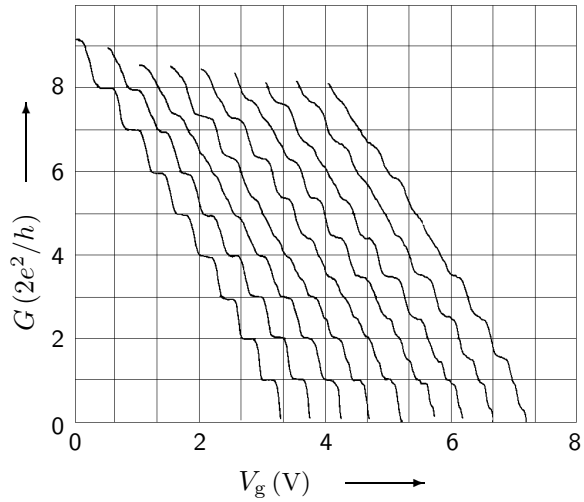

Fig. 68: The evolution of additional quantized conductance plateaux with increasing bias is illustrated. The source-drain bias is increased in steps of 0.5 mV and the measurements are taken at 30 mK and at a finite magnetic field of 0.5 T [90P].

[91B3]. For moderate applied bias the characteristics of in-plane gate devices can be reasonably modelled using a parabolic tunneling barrier and a linear potential drop along the channel. In-plane gate geometries have also been utilized in spectroscopic investigations of the 2DEG in which the QPC is defined [91B4, 92B1]. In these studies the differential resistance in the non-linear regime is numerically differentiated to obtain the second derivative $\mathrm{d}^2V/\mathrm{d}I^2$ as a function of the applied bias. In 3D metallic systems this second derivative can be shown to be proportional to the Eliashberg form of the electron-phonon interaction [80J]. Typical data for a variety of gate voltages are shown in Figs. 71 and 72. The observed structures in the second derivative lie close to the maxima of the phonon density of states, as indicated by the arrows in Figs. 71 and 72, and suggest strongly that this is a viable method to investigate electron-phonon scattering in 2D systems. Furthermore, the observed structure is essentially independent of the Fermi energy of the 2DEG, and can be continuously tuned within the spectroscopic region via a variation of the channel width. The condition required for the validity of the point contact spectroscopy is that the channel width be less than the electronic mean free path, and as expected the structure in the second derivative becomes increasingly more pronounced as the width is reduced.

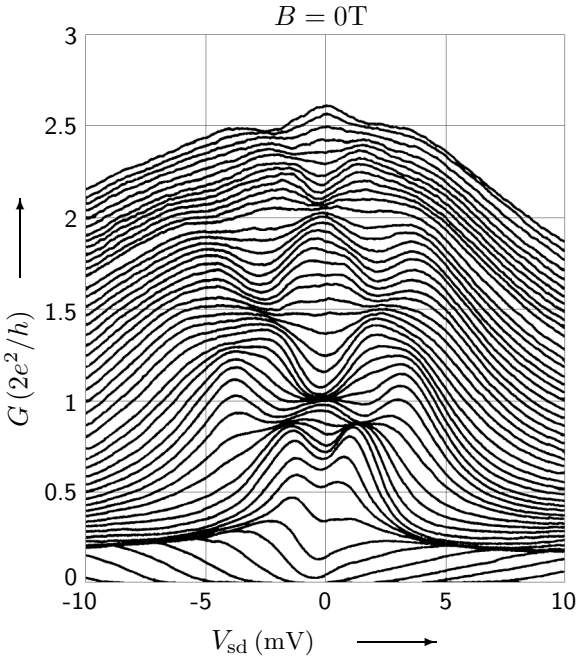

Fig. 69: The differential conductance is plotted as a function of the applied source-drain bias for different gate voltages ($\Delta V_g = 25$ mV) [91P1].

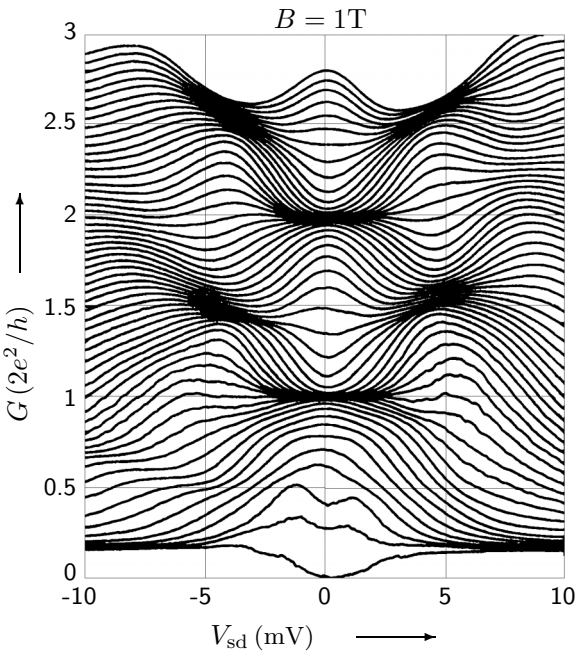

Fig. 70: The differential conductance is plotted as a function of the applied source-drain bias in a perpendicular magnetic field of 1 T. The gate voltage variation between traces is 25 mV as before [91P1].

The possibility of extracting the intersubband spacing through measurements of the non-linearity of the conductance has been successfully exploited to investigate the nature of the confining potential in QPC devices fabricated on both shallow and conventional heterostructure material [94F]. Both the saddle-point confining potential [90B2] as well as a modified version thereof which accounts for the self-consistent potential contribution resulting from the finite electron density in the QPC channel have been considered. The measured non-linear behaviour was compared with that expected from simple analytical considerations; for small electron densities the saddle-point potential with parabolic lateral confinement fitted the data best while for higher densities with a larger number of occupied subbands the self-consistent confining potential yielded better agreement, as expected from more detailed considerations [88L1, 89W2].

None of the above models explicitly considers the influence of the source-drain bias upon the QPC geometry in the high-bias regime, despite the fact that the applied bias can become comparable, or at least of the same order of magnitude, as the applied gate voltage. It is therefore to be expected, as discussed above (see Section 3.1.10 [89L1]) that the channel geometry will be significantly modified in the non-linear regime [94H]. This effect is most pronounced when the difference between the positive and negative polarities of source-drain bias is considered as illustrated in Figs. 73 and 74. Assuming a simple analytical confining potential and that, at least in the high-bias regime, the electric field strength is maximal where the channel width is narrowest, as expected in the diffusive regime, the non-linear characteristics can be readily computed as shown in Fig. 74. This model reproduces well the absence of a saturation of the current-voltage characteristics in the very high-bias regime but cannot reproduce the lack of antisymmetry typically seen in the data. In the very high-bias limit the self-consistent influence of the applied source-drain bias upon the QPC geometry must be considered. A correct theoretical formulation involves the solution of an integro-differential equation [89L1] and has yet to be solved exactly. An alternative approach lies in the use of an effective gate voltage where the channel width is not purely given by the applied gate voltage but also by the position dependent voltage drop along the length of

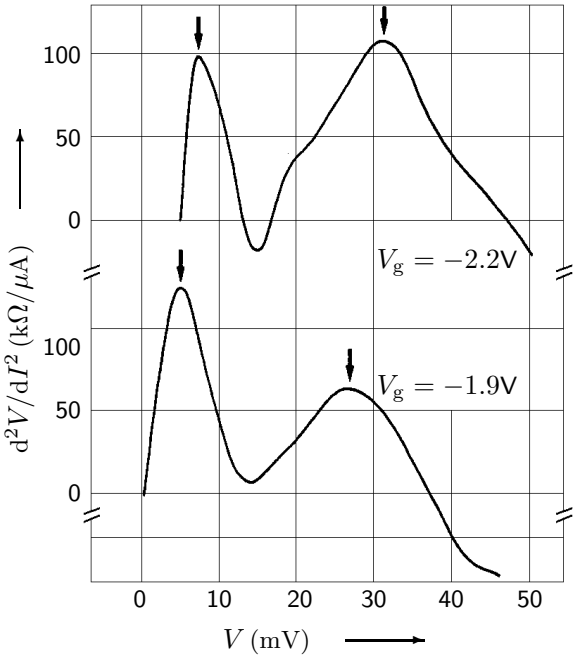

Fig. 71: The second derivative of the current-voltage characteristics of an in-plane gate QPC device is shown as a function of the applied bias for a number of different gate voltages [91B4]. See also Fig. 72.

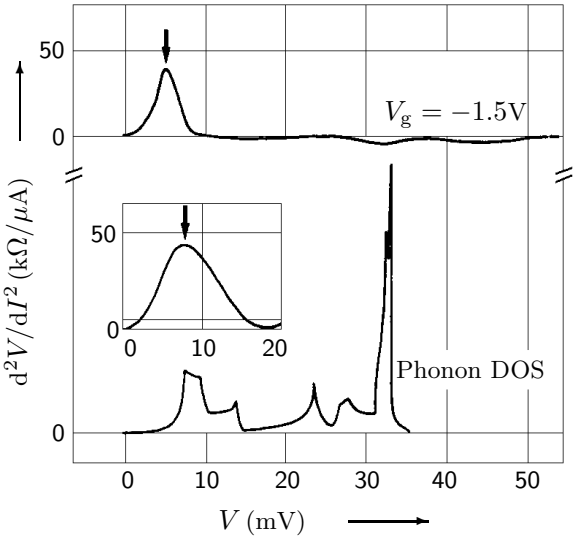

Fig. 72: As in Fig. 71 the second derivative of the current voltage characteristics is plotted as a function of the applied bias. Also shown is the phonon density of states for GaAs [91B4]. The inset shows results for larger E_F.

the channel in the high-bias regime. The results of such a calculation are presented in Fig. 75 and show a good quantitative and qualitative agreement between the experimental data and the theoretical model.

Interestingly, for strong lateral confining potentials the introduction of an effective gate voltage leads to the prediction of a negative differential conductance for large positive source-drain bias, which has to date not been observed in a simple QPC device. Negative differential conductance has however been observed in related, quantum waveguide geometries [92W, 94B] where it is believed to be associated with hot electron transport through charge islands. In the open geometry of the original experiment [92W] the charge island was formed artificially through the lithographic definition of a quantum dot type geometry. The S-type negative differential conductivity observed occurs at high source-drain bias when the excess kinetic energy of the hot electrons is sufficient to raise the ambient temperature in the charge island such that thermionic emission is dramatically enhanced. Such effects have also been observed [94B] in a quantum waveguide geometry, where the channel length was, in contrast to conventional QPC devices, formed by laterally overlapping gate electrodes such that the channel width was well-defined, independent of channel length. The fabricated devices all showed pronounced conductance quantization and, after illumination at low temperatures, a significant S-type negative differential conductivity (see Fig. 76). Annealing the devices at 120 K for 12 hours was sufficient to restore the original QPC like current-voltage characteristics, suggesting that the observed current instabilities are associated with the light induced occupation of DX centres in the AlGaAs layer of the heterostructure material. Again it is postulated that the negative differential conductance is associated with the hot electron transport through charge islands defined by the inhomogeneous potential distribution resulting from ionized DX centres. This explains also the observation of more than one S-type instability in the observed characteristics.

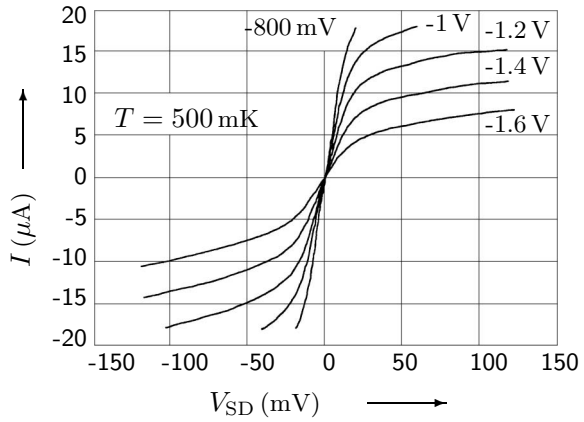

Fig. 73: Typical measurements of the current-voltage characteristics of a ballistic QPC are presented. Ten subbands are occupied at a gate-voltage of $V_g = -800\,mV$ and only two subbands contribute to the current at $V_g = -1.6\,V$ [94H].

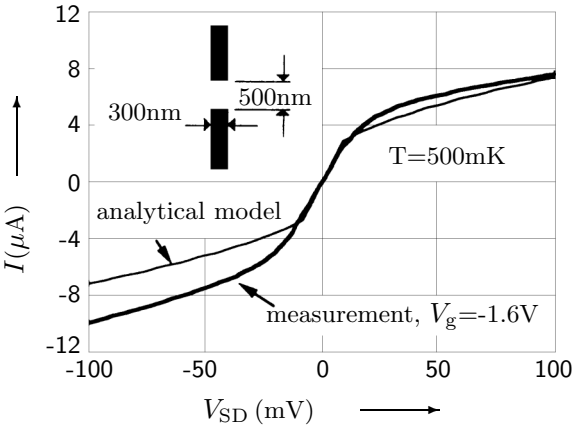

Fig. 74: The measured current-voltage characteristic for $V_g = -1.6\,V$ is compared with the results of a simple analytical calculation which assumes a classical field distribution within a diffusive model. The observed asymmetry can be accounted for by including an additional position dependent effective gate voltage [94H].

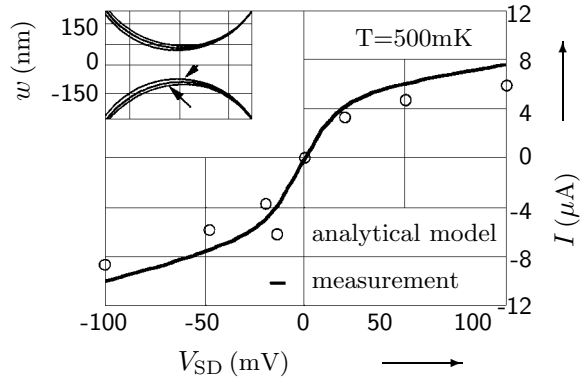

Fig. 75: The calculated current-voltage characteristics in the high-bias regime determined using a self-consistent approach which accounts for the interplay between source-drain bias and gate-voltage [94H].

3.11 Thermal transport properties

The oscillations in the thermopower discussed in Section 3.1.13 above have been indirectly observed [90M3] via the measurement of a transverse voltage between two asymmetrically tuned QPCs connected to the same 2D resevoir. The experimental setup is shown in the inset of Fig. 77 where the transverse voltage (i.e. $V_1 - V_2$) is plotted as a function of the gate bias applied to one QPC electrode pair. The observed oscillations of the transverse voltage are clearly correlated with the steps between quantized plateaux. The DC current flowing through the 2D bulk sandwiched between the two QPC detectors causes electron heating within the bulk and gives rise to a shifted Fermi distribution. The measured transverse voltage is even in the current and has an approximately quadractic current dependence as expected for Joule heating within the 2DEG. The comparison with theory (see Fig. 78) was derived under the assumption that there is no net current between 2DEG and the QPC reservoirs. This zero transmission condition allows the chemical potential difference to be directly related to the temperature difference and hence the transverse voltage to be determined. Only when the transmission has a significant energy dependence is a nonzero transverse voltage expected, as indeed found at the transitions between quantized plateaux. Comparable measurements have been subsequently reported [92Y2] and the magnitude of the thermopower maxima compared with the theoretical prediction $S_n^{max} \sim -60/(n + 1/2)\mu V/K$. Typical measurements were within about 20 % of the predicted values for low index plateaux, and for small currents the agreement

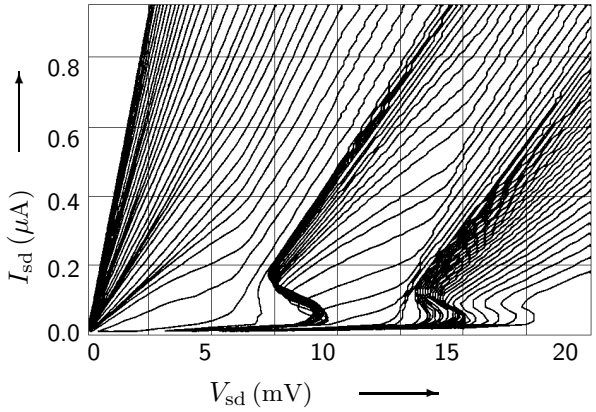

Fig. 76: The current-voltage characteristics of the quantum waveguide geometry with length 0.1 μm are plotted for gate-voltage increments of ΔV_g = 20 mV [94B].

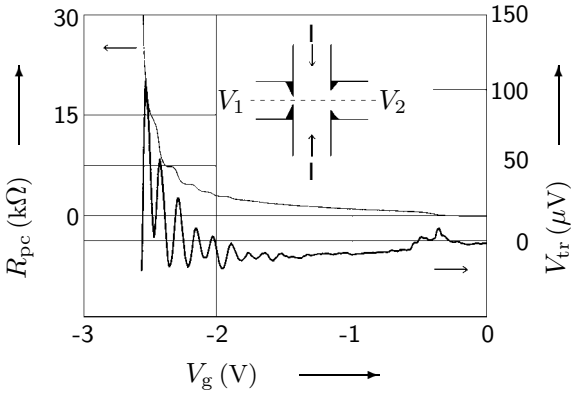

Fig. 77: The transverse voltage $V_1 - V_2$ (see inset) is plotted as a function of the gate bias applied to the electrode pair defining QPC_1. Also shown is the resistance of QPC_1. Both measurments were performed at T = 1.65 K for a current $I = 5\,\mu$A and $V_{g2} = -2.0$ V [90M3].

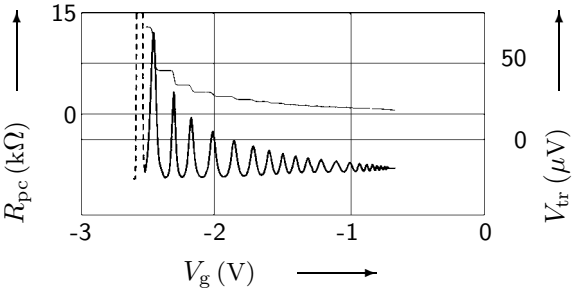

Fig. 78: The calculated values for the transverse voltage and QPC resistance for the experimental parameters defined in Fig. 77 [90M3].

improved to within 10 %.

The above analysis can, of course, be exploited to infer the temperature difference between two reservoirs connected by a ballistic QPC providing a reliable estimate for the thermopower is known. Such a technique has been used [92M2, 92vH] to investigate the quantum mechanical nature of both the thermal conductance and Peltier coefficient. As predicted from the Kelvin-Onsager relations, quantum size effects in the thermopower S should be accompanied by a change in the Peltier coefficient $\Pi = ST$. This effect has been investigated in a QPC where the thermal current is inferred from the measurement of thermovoltages in source and drain reservoirs, and can be directly compared with the subsequently measured thermovoltage between source and drain contacts. Good quantitative agreement was found with an assumed thermopower $S = -k_B \ln 2/(n + 1/2)e \approx -40\,\mu$V/K when the QPC is tuned to the middle of the n-th plateau. Similarly, the thermal conductivity was measured by locally heating the source reservoir and measuring the accompanying thermal current. The thermal conductivity showed structure reminiscent of the QPC conductance, as may be expected from the Wiedemann-Franz relation $\kappa \approx L_0 TG$ where $L_0 \equiv k_B^2 \pi^2/3e^2$ is the Lorenz number and G the conductance.

3.12 Coulomb blockade

Although Coulomb-blockade effects are not expected in the conductance of an ideal QPC, a number of reports related to such effects have been published [91dG, 92N1]. Presumably, these observations

are related to QPC geometries which, by virtue of their fabrication, are more likely to contain an isolated conducting segment connected to the source and drain reservoirs via tunneling contacts. In a Si-QPC [91dG], defined used a stack-gated technique (see Section 2.1), periodic oscillations in the conductance as a function of applied gate bias are observed shortly before the device pinches off. Both the gate characteristic as well as the source-drain characteristic are entirely consistent with an interpretation based upon Coulomb effects. In an etched QPC geometry [92N1], which could be tuned with side-gates defined in the same δ-doped layer, the observed current-voltage charcteristics showed a Coulomb gap of roughly 5 mV. The modulation of the blockade via the side-gates could be demonstrated, and quasi-periodic structure in the conductance of the device was found. However, the exact device geometry is difficult to determine with the experimental data presented and it is speculated that the long channel contains several barriers and conducting islands, and should therefore show the so-called stochastic Coulomb blockade.

3.13 Superconducting QPCs

Superconducting QPCs have been fabricated in high-mobility InAs layers, where Nb contacts serve as ohmic contacts to the high-mobility electron gas which can be tuned via split-gate electrodes [95T1]. In such systems measurements of the normalized differential resistance have been performed as a function of gate electrode bias. At the Nb/2DEG interface the carriers can be transmitted, reflected or indeed Andreev reflected, the latter process resulting in an excess current. The gate voltage dependent characteristics show that, in the absence of a narrow channel the device characteristics at $V = 0$ show an increased differential resistance. As the QPC is defined the differential resistance at zero bias decreases, and the excess current is attributed to Andreev reflected holes which are focused towards the QPC. Related measurements of coherent Andreev backscattering have subsequently been reported [97dH] in the disordered limit.

Similar devices have been employed [96T2] to investigate the nature of the critical current in superconducting QPCs. In Fig. 79 both the critical current and conductance are plotted as a function of the applied gate-bias. The observed conductance quantization is modified and the steps in conductance are somewhat larger than in the normal case. Single and multiple Andreev reflections will modify the quantization but, for the geometry considered, no theory has addressed this problem so far. The critical current also shows steps of magntiude 5 nA which, whilst considerably smaller than expected, confirm at least qualitatively the theory discussed in Section 3.1.14 above.

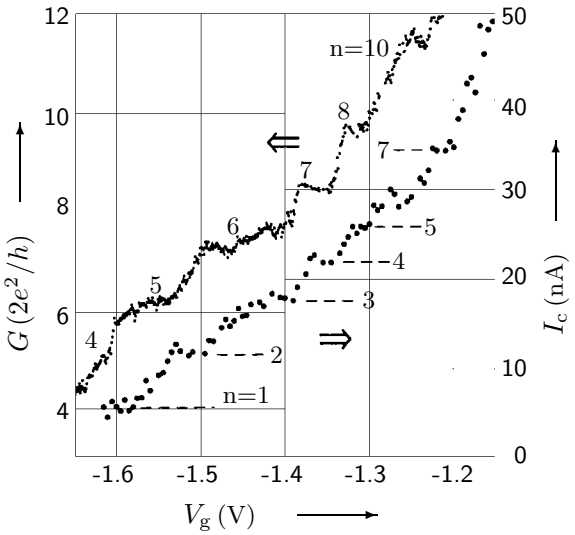

Fig. 79: The conductance and critical current of a superconducting QPC are plotted as a function of the applied gate bias [96T2].

3.14 Effect of radiation

The influence of alpha particle radiation upon the conductance characteristics has been invetsigated at low temperatures [93T]. The incident radiation penetrates roughly 20 μm into the semiconductor heterostructure and creates electron-hole pairs as well as ionized inpurities. The latter create a local potential minimum which can be clearly seen in the conductance characteristics of the QPC device when the impinging alpha particle hits within a distance of roughly 5 μm from the QPC. The influence of the potential minima is such that the conductance is briefly enhanced by as much as $2e^2/h$, especially in the transition region between plateaux, and then decays on a time scale of approximately 10 s.

3.15 References for Section 3

[56HB] Hanbury Brown, R., Twiss, R.Q.: Nature **177** (1956) 27.

[80J] Jansen, A.G.M., van Gelder, A.P., Wyder, P.: J. Phys. C **13** (1980) 6073.

[86L] Laux, S.E., Stern, F.: Appl. Phys. Lett. **49** (1986) 91.

[86T] Thornton, T.J., Pepper, M., Ahmed, H., Andrews, D., Davies, G.J.: Phys. Rev. Lett. **56** (1986) 1198.

[87G] Grimzewski, J.K., Möller, R.: Phys. Rev. B **36** (1987) 1284.

[87R] Roukes, M.L., Scherer, A., Allen, S.J., Craighead, H.G., Ruthen, R.M., Beebe, E.D., Harbison, J.P.: Phys. Rev. Lett. **59** (1987) 3011.

[88B1] Beenakker, C.W.J., van Houten, H., van Wees, B.J.: Europhys. Lett. **7** (1988) 359.

[88B2] Berggren, K.-F., Roos, G., van Houten, H.: Phys. Rev. B **37** (1988) 10188.

[88G1] Glazman, L.I., Khaetskiĭ, A.V.: JETP Lett. **48** (1988) 591.

[88G2] Glazman, L.I., Lesovik, G.B., Khmel'nitskiĭ, D.E., Shekhter, R.I.: JETP Lett. **48** (1988) 238.

[88I] Isawa, Y.: J. Phys. Soc. Jpn. **57** (1988) 3457.

[88J] Johnston, R., Schweitzer, L.: J. Phys. C **21** (1988) L861.

[88K1] Kirczenow, G.: Phys. Rev. B **38** (1988) 10958.

[88K2] Kirczenow, G.: Solid. State. Comm. **68** (1988) 715.

[88K3] Kopley, T.E., McEuen, P.L., Wheeler, R.G.: Phys. Rev. Lett. **61** (1988) 1654.

[88K4] Kramer, B., Mašek, J.: J. Phys. C **21** (1988) L1147.

[88L1] Laux, S.E., Frank, D.J., Stern, F.: Surf. Sci. **196** (1988) 101.

[88L2] Levinson, I.B.: JETP Lett. **48** (1988) 301.

[88vH] van Houten, H., van Wees, B.J., Mooij, J.E., Beenakker, C.W.J., Williamson, J.G., Foxon, C.T.: Europhys. Lett. **5** (1988) 721.

[88vL] van Loosdrecht, P.H.M., Beenakker, C.W.J., van Houten, H., Williamson, J.G., van Wees, B.J., Mooij, J.E., Foxon, C.T., Harris, J.J.: Phys. Rev. B **38** (1988) 10162.

[88vW1] van Wees, B.J., van Houten, H., Beenakker, C.W.J., Williamson, J.G., Kouwenhoven, L.P., van der Marel, D., Foxon, C.T.: Phys. Rev. Lett. **60** (1988) 848.

[88vW2] van Wees, B.J., Kouwenhoven, L.P., van Houten, H., Beenakker, C.W.J., Mooij, J.E., Foxon, C.T., Harris, J.J.: Phys. Rev. B **38** (1988) 3625.

[88W1] Wharam, D.A., Thornton, T.J., Newbury, R., Pepper, M., Ahmed, H., Frost, J.E.F., Hasko, D.G., Peacock, D.C., Ritchie, D.A., Jones, G.A.C.: J. Phys. C **21** (1988) L209.

[88W2] Wharam, D.A., Pepper, M., Ahmed, H., Frost, J.E.F., Hasko, D.G., Peacock, D.C., Ritchie, D.A., Jones, G.A.C.: J. Phys. C **21** (1988) L887.

[88W3] Widom, A., Tao, R.: J. Phys. C **21** (1988) L1061.

[89B1] Bagwell, P.F., Orlando, T.P.: Phys. Rev. B **40** (1989) 1456.

[89B2] Baranger, H.U., Stone, A.D.: Phys. Rev. Lett. **63** (1989) 414.

[89B3] Beenakker, C.W.J., van Houten, H.: Phys. Rev. B **39** (1989) 10445.

[89B4] Beton, P.H., Snell, B.R., Main, P.C., Neves, A.J.M., Owers-Bradley, J.R., Eaves, L., Henini, M., Hughes, O.H., Beaumont, S.P., Wilkinson, C.D.W.: J. Phys.: Condens. Matter **1** (1989) 7505.

[89B5] Brown, R.J., Kelly, M.J., Pepper, M., Ahmed, H., Hasko, D.G., Peacock, D.C., Frost, J.E.F., Ritchie, D.A., Jones, G.A.C.: J. Phys.: Condens. Matter **1** (1989) 6285.

[89G1] Glazman, L.I., Khaetskiĭ, A.V.: Europhys. Lett. **9** (1989) 263.

[89G2] Glazman, L.I., Khaetskiĭ, A.V.: J. Phys.: Condens. Matter **1** (1989) 5005.

[89H2] Haanappel, E.G., van der Marel, D.: Phys. Rev. B **39** (1989) 5484.

[89H3] He, S., Das Sarma, S.: Phys. Rev. B **40** (1989) 3379.

[89K1] Kawabata, A.: J. Phys. Soc. Jpn. **58** (1989) 372.

[89K2] Kelly, M.J.: J. Phys.: Condens. Matter **1** (1989) 7643.

[89K3] Kelly, M.J., Brown, R.J., Smith, C.G., Wharam, D.A., Pepper, M., Ahmed, H., Hasko, D.G., Peacock, D.C., Frost, J.E.F., Newbury, R., Ritchie, D.A., Jones, G.A.C.: Electron. Lett. **25** (1989) 992.

[89K4] Kirczenow, G.: Phys. Rev. Lett. **62** (1989) 1920.

[89K5] Kirczenow, G.: J. Phys.: Condens. Matter **1** (1989) 305.

[89K6] Kouwenhoven, L.P., van Wees, B.J., Harmans, C.J.P.M., Williamson, J.G., van Houten, H., Beenakker, C.W.J., Foxon, C.T., Harris, J.J.: Phys. Rev. B **39** (1989) 8040.

[89L1] Levinson, I.B.: Sov. Phys. JETP **68** (1989) 1257.

[89M] Mašek, J., Kramer, B.: Z. Phys. B **75** (1989) 37.

[89S1] Shikin, V.B.: JETP Lett. **50** (1989) 167.

[89S2] Sivan, U., Heiblum, M., Umbach, C.P.: Phys. Rev. Lett. **63** (1989) 992.

[89S3] Smith, C.G., Pepper, M., Ahmed, H., Frost, J.E.F., Hasko, D.G., Newbury, R., Peacock, D.C., Ritchie, D.A., Jones, G.A.C.: J. Phys.: Condens. Matter **1** (1989) 9035.

[89S4] Smith, C.G., Pepper, M., Newbury, R., Ahmed, H., Hasko, D.G., Peacock, D.C., Frost, J.E.F., Ritchie, D.A., Jones, G.A.C., Hill, G.: J. Phys.: Condens. Matter **1** (1989) 6763.

[89S5] Streda, P.: J. Phys.: Condens. Matter **1** (1989) 1025.

[89S6] Szafer, A., Stone, A.D.: Phys. Rev. Lett. **62** (1989) 300.

[89T] Timp, G., Behringer, R.E., Sampere, S., Cunningham, J.E., Howard, R.E.: in Nanostructure Physics and Fabrication, Academic Press (1989) 331 331.

[89vdM] van der Marel, D., Haanappel, E.G.: Phys. Rev. B **39** (1989) 7811.

[89vH] van Houten, H., Beenakker, C.W.J., Williamson, J.G., Broekaart, M.E.I., van Loosdrecht, P.H.M., van Wees, B.J., Mooij, J.E., Foxon, C.T., Harris, J.J.: Phys. Rev. B **39** (1989) 8556.

[89vW1] van Wees, B.J., Kouwenhoven, L.P., Harmans, C.J.P.M., Williamson, J.G., Timmering, C.E., Broekaart, M.E.I., Foxon, C.T., Harris, J.J.: Phys. Rev. Lett. **62** (1989) 2523.

[89vW2] van Wees, B.J., Willems, E.M.M., Harmans, C.J.P.M., Beenakker, C.W.J., van Houten, H., Williamson, J.G., Foxon, C.T., Harris, J.J.: Phys. Rev. Lett. **62** (1989) 1181.

[89vW3] van Wees, B.J., Willems, E.M.M., Kouwenhoven, L.P., Harmans, C.J.P.M., Williamson, J.G., Foxon, C.T., Harris, J.J.: Phys. Rev. B **39** (1989) 8066.

[89W1] Weisz, J.F., Berggren, K.-F.: Phys. Rev. B **40** (1989) 1325.

[89W2] Wharam, D.A., Ekenberg, U., Pepper, M., Ahmed, H., Frost, J.E.F., Hasko, D.G., Peacock, D.C., Ritchie, D.A., Jones, G.A.C.: Phys. Rev. B **39** (1989) 6283.

[89W3] Wharam, D.A., Pepper, M., Ahmed, H., Frost, J.E.F., Hasko, D.G., Peacock, D.C., Ritchie, D.A., Jones, G.A.C.: J. Phys.: Condens. Matter **1** (1989) 3369.

[90B1] Brown, R.J., Pepper, M., Ahmed, H., Hasko, D.G., Ritchie, D.A., Frost, J.E.F., Peacock, D.C., Jones, G.A.C.: J. Phys.: Condens. Matter **2** (1990) 2105.

[90B2] Büttiker, M.: Phys. Rev. B **41** (1990) 7906.

[90G2] Glazman, L.I., Jonson, M.: Phys. Rev. B **41** (1990) 10686.

[90M1] McEuen, P.L., Alphenaar, B.W., Wheeler, R.G., Sacks, R.N.: Surf. Sci. **229** (1990) 312.

[90M2] Molenkamp, L.W., Staring, A.A.M., Beenakker, C.W.J., Eppenga, R., Timmering, C.E., Williamson, J.G., Harmans, C.J.P.M., Foxon, C.T.: Phys. Rev. B **41** (1990) 1274.

[90M3] Molenkamp, L.W., van Houten, H., Beenakker, C.W.J., Eppenga, R., Foxon, C.T.: Phys. Rev. Lett. **65** (1990) 1052.

[90P] Patel, N.K., Martín-Moreno, L., Pepper, M., Newbury, R., Frost, J.E.F., Ritchie, D.A., Jones, G.A.C., Janssen, T.J.B.M., Singleton, J., Perenboom, J.A.A.J.: J. Phys.: Condens. Matter **2** (1990) 7247.

[90T1] Tekman, E., Ciraci, S.: Phys. Rev. B **42** (1990) 9098.

[90W2] Williamson, J.G., Timmering, C.E., Harmans, C.J.P.M., Harris, J.J., Foxon, C.T.: Phys. Rev. B **42** (1990) 7675.

[90W3] Williamson, J.G., van Houten, H., Beenakker, C.W.J., van Wees, B.J., Foxon, C.T.: Phys. Rev. B. **41** (1990) 1207.

[90Y1] Yacoby, A., Imry, Y.: Phys. Rev. B **41** (1990) 5341.
[91B1] Beenakker, C.W.J., van Houten, H.: Phys. Rev. Lett. **66** (1991) 3056.
[91B2] Behringer, R.E., Timp, G., Baranger, H.U., Cunningham, J.E.: Phys. Rev. Lett. **66** (1991) 930.
[91B3] Bever, T., Wieck, A.D., von Klitzing, K., Ploog, K.: Phys. Rev. B **44** (1991) 3424.
[91B4] Bever, T., Wieck, A.D., von Klitzing, K., Ploog, K., Wyder, P.: Phys. Rev. B **44** (1991) 6507.
[91dG] de Graaf, C., Caro, J., Radelaar, S., Lauer, V., Heyers, K.: Phys. Rev. B **44** (1991) 9072.
[91L1] Laughton, M.J., Barker, J.R., Nixon, J.A., Davies, J.H.: Phys. Rev. B **44** (1991) 1150.
[91M] Montie, E.A., Cosman, E.C., t Hooft, G.W., van der Mark, M.B., Beenakker, C.W.J.: Nature **350** (1991) 594.
[91N] Nixon, J.A., Davies, J.H., Baranger, H.U.: Phys. Rev. B **43** (1991) 12638.
[91P1] Patel, N.K., Nicholls, J.T., Martín-Moreno, L., Pepper, M., Frost, J.E.F., Ritchie, D.A., Jones, G.A.C.: Phys. Rev. B **44** (1991) 13549.
[91P2] Patel, N.K., Nicholls, J.T., Martín-Moreno, L., Pepper, M., Frost, J.E.F., Ritchie, D.A., Jones, G.A.C.: Phys. Rev. B **44** (1991) 10973.
[91P3] Proetto, C.R.: Phys. Rev. B **44** (1991) 9096.
[91T] Tekman, E., Ciraci, S.: Phys. Rev. B **43** (1991) 7145.
[91vW] van Wees, B.J., Kouwenhoven, L.P., Willems, E.M.M., Harmans, C.J.P.M., Mooij, J.E., van Houten, H., Beenakker, C.W.J., Williamson, J.G., Foxon, C.T.: Phys. Rev. B **43** (1991) 12431.
[91Y] Yamada, S., Yamamoto, M.: Phys. Rev. B **43** (1991) 9369.
[91Z] Zwerger, W., Bönig, L., Schönhammer, K.: Phys. Rev. B **43** (1991) 6434.
[92B1] Bever, T., Wieck, A.D., von Klitzing, K., Ploog, K., Wyder, P.: Helv. Phys. Acta **65** (1992) 313.
[92C1] Castaño, E., Kirczenow, G.: Phys. Rev. B **45** (1992) 1514.
[92F1] Fedichkin, L., Fedirko, V.A., V'yurkov, V.V.: Lith. J. Phys. **32** (1992) 53.
[92F2] Fedirko, V.A., Ryzhii, V.I., V'yurkov, V.V.: Soviet J. Low Temp. Phys. **18** (1992) 651.
[92F3] Furusaki, A., Takayanagi, H., Tsukada, M.: Phys. Rev. B **45** (1992) 10563.
[92H2] Hekking, F.W.J., Nazarov, Yu.V., Schön, G.: Europhys. Lett. **20** (1992) 255.
[92K] Kane, C.L., Fisher, M.P.A.: Phys. Rev. Lett. **68** (1992) 1220.
[92M1] Molenkamp, L.W., Brugmans, M.J.P., van Houten, H., Foxon, C.T.: Semicond. Sci. Technol. **7** (1992) B228.
[92M2] Molenkamp, L.W., Gravier, T., van Houten, H., Buijk, O.J.A., Mabesoone, M.A.A., Foxon, C.T.: Phys. Rev. Lett. **68** (1992) 3765.
[92MM] Martín-Moreno, L., Nicholls, J.T., Patel, N.K., Pepper, M.: J. Phys.: Condens. Matter **4** (1992) 1323.
[92N1] Nakazato, K., Thornton, T.J., White, J., Ahmed, H.: Appl. Phys. Lett. **61** (1992) 3145.
[92N2] Neves, A.J.M., Main, P.C., Langerak, C.J.G.M, Beton, P.H., Eaves, L., Henini, M., Hughes, O.H., Beaumont, S.P., Wilkinson, C.D.W.: Semicond. Sci. Technol. **7** (1992) B279.
[92O] Okada, M., Saito, M., Takatsu, M., Schmidt, P.E., Kosemura, K., Yokoyama, N.: Semicond. Sci. Technol. **7** (1992) B223.
[92P1] Palacios, J.J., Tejedor, C.: Phys. Rev. B **45** (1992) 13725.
[92P2] Patel, N.K., Martín-Moreno, L., Nicholls, J.T., Pepper, M., Frost, J.E.F., Ritchie, D.A., Jones, G.A.C.: Superlattices and Microstructures **11** (1992) 233.
[92S1] Snider, G.L., Tan, I.-H., Miller, M.S., Rooks, M.J., Hu, E.L.: Superlattices and Microstructures **11** (1992) 297.
[92S2] Saito, M., Takatsu, M., Okada, M., Yokoyama, N.: Phys. Rev. B **46** (1992) 13220.
[92S3] Spector, J., Weiner, J.S., Störmer, H.L., Baldwin, K.W., Pfeiffer, L.N., West, K.W.: Surf. Sci. **263** (1992) 240.

[92T2] Takagaki, Y., Ferry, D.K.: Phys. Rev. B **45** (1992) 13494.
[92T3] Takagaki, Y., Ferry, D.K.: Phys. Rev. B **45** (1992) 12152.
[92vH] van Houten, H., Molenkamp, L.W., Beenakker, C.W.J., Foxon, C.T.: Semicond. Sci. Technol. **7** (1992) B215.
[92W] Wu, J.C., Wybourne, M.N., Berven, C., Goodnick, S.M., Smith, D.D.: Appl. Phys. Lett. **61** (1992) 2425.
[92Y1] Yamada, S.: Phys. Rev. B **45** (1992) 14162.
[92Y2] Yamada, S., Yamamoto, M.: Semicond. Sci. Technol. **7** (1992) B289.
[92Y3] Yamada, S., Yamamoto, M., Aihara, K.: Surf. Sci. **263** (1992) 265.
[93B] Bogachek, E.N., Jonson, M., Shekhter, R.I., Swahn, T.: Phys. Rev. B **47** (1993) 16635.
[93H1] He, S., Das Sarma, S.: Phys. Rev. B **48** (1993) 4629.
[93M2] Maslov, D.L., Barnes, C., Kirczenow, G.: Phys. Rev. Lett. **70** (1993) 1984.
[93T] Taboryski, R., Baklanov, K., Lindelof, P.E.: Phys. Rev. Lett. **70** (1993) 2475.
[93X] Xu, H.: Phys. Rev. B **48** (1993) 8878.
[93Y] Yao, J., Chen, H.: Z. Phys. B **92** (1993) 341.
[94B] Berven, C., Wybourne, M.N., Ecker, A., Goodnick, S.M.: Phys. Rev. B **50** (1994) 14639.
[94C] Chu, C.S., Chou, M.-H.: Phys. Rev. B **50** (1994) 14212.
[94F] Frost, J.E.F., Berggren, K.-F., Pepper, M., Grimshaw, M.P., Ritchie, D.A., Churchill, A.C., Jones, G.A.C.: Phys. Rev. B **49** (1994) 11500.
[94H] Heinzel, T., Wharam, D.A., de Aguiar, F.M., Kotthaus, J.P., Böhm, G., Klein, W., Tränkle, G., Weimann, G.: Semicond. Sci. Technol. **9** (1994) 1220.
[94K1] Kogan, S.M.: Phys. Rev. B **50** (1994) 17230.
[94L1] Larkin, I.A., Sukhorukov, E.V.: Phys. Rev. B **49** (1994) 5498.
[94M] Maaø, F.A., Zozulenko, I.V., Hauge, E.H.: Phys. Rev. B **50** (1994) 17320.
[94MR] Marigliano Ramaglia, V., Ventriglia, F., Zucchelli, G.P.: J. Phys. I France **4** (1994) 1743.
[94S] Saito, M., Usuki, T., Okada, M., Futatsugi, T., Kiehl, R.A., Yokoyama, N.: Appl. Phys. Lett. **65** (1994) 3087.
[94U] Usuki, T., Takatsu, M., Kiehl, R.A., Yokoyama, N.: Phys. Rev. B **50** (1994) 7615.
[94W] Wald, K.R., Kouwenhoven, L.P., McEuen, P.L., van der Vaart, N.C., Foxon, C.T.: Phys. Rev. Lett. **73** (1994) 1011.
[94Z] Zagoskin, A.M., Shekhter, R.I.: Phys. Rev. B **50** (1994) 4909.
[95E] Eiles, T.M., Simmons, J.A., Sherwin, M.E., Klem, J.F.: Phys. Rev. B **52** (1995) 10756.
[95F] Fendley, P., Ludwig, A.W.W., Saleur, H.: Phys. Rev. B **52** (1995) 8934.
[95K] Krans, J.M., Muller, C.J., van der Post, N., Postma, F.R., Sutton, A.P., Todorov, T.N., van Ruitenbeek, J.M.: Phys. Rev. Lett. **74** (1995) 2146.
[95M1] Malysheva, L.I., Onipko, A.I.: J. Phys.: Condens. Matter **7** (1995) 3597.
[95M2] Maslov, D.L., Stone, M.: Phys. Rev. B **52** (1995) R5539.
[95M3] Müller, F., Lengeler, B., Schäpers, T., Appenzeller, J., Förster, A., Klocke, T., Lüth, H.: Phys. Rev. B **51** (1995) 5099.
[95P] Ponomarenko, V.V.: Phys. Rev. B **52** (1995) R8666.
[95T1] Takayanagi, H., Akazaki, T.: Phys. Rev. B **52** (1995) R8633.
[95T2] Takeuchi, K., Hisamoto, D., Yamashita, H.: Appl. Phys. Lett. **66** (1995) 1776.
[95T4] Többen, D., Wharam, D.A., Abstreiter, G., Kotthaus, J.P., Schäffler, F.: Phys. Rev. B **52** (1995) 4704.
[95U] Usuki, T., Saito, M., Takatsu, M., Kiehl, R.A., Yokoyama, N.: Phys. Rev. B **52** (1995) 8244.
[95Z] Zagoskin, A.M., Rashkeev, S.N., Shekhter, R.I., Wendin, G.: J. Phys.: Condens. Matter **7** (1995) 6253.
[96A] Alekseev, A.Y., Cheianov, V.V., Frölich, J.: Phys. Rev. B **54** (1996) R17320.
[96C] Christen, T., Büttiker, M.: Phys. Rev. Lett. **77** (1996) 143.

[96K1] Kasai, H., Kakuda, T., Okiji, A.: Surf. Sci. **363** (1996) 428.
[96K2] Kawabata, A.: J. Phys. Soc. Jpn. **65** (1996) 30.
[96K3] Khaetskiĭ, A.V., Nazarov, Yu.V., Bauer, G.E.W.: Surf. Sci. **361/362** (1996) 67.
[96L1] Liang, C.-T., Smith, C.G., Mace, D.R., Nicholls, J.T., Frost, J.E.F., Simmons, M.Y., Hamilton, A.R., Ritchie, D.A., Pepper, M.: Phys. Rev. B **53** (1996) 7596.
[96L2] Liang, C.-T., Smith, C.G., Mace, D.R., Nicholls, J.T., Frost, J.E.F., Simmons, M.Y., Hamilton, A.R., Ritchie, D.A., Pepper, M.: Surf. Sci. **361/362** (1996) 71.
[96O] Oreg, Y., Finkel'stein, A.M.: Phys. Rev. B **54** (1996) 14265.
[96T2] Takayanagi, H., Akazaki, T., Nitta, J.: Surf. Sci. **361/362** (1996) 298.
[96T3] Thomas, K.J., Nicholls, J.T., Simmons, M.Y., Pepper, M., Mace, D.R., Ritchie, D.A.: Phys. Rev. Lett. **77** (1996) 135.
[96W] Wang, C.-K., Berggren, K.-F.: Phys. Rev. B **54** (1996) 14257.
[96Y] Yacoby, A., Stormer, H.L., Wingreen, N.S., Pfeiffer, L.N., Baldwin, K.W., West, K.W.: Phys. Rev. Lett. **77** (1996) 4612.
[97C] Chen, H., Shi, Y., Yu, J., Zhu, J.-L., Kawazoe, Y.: Phys. Rev. B **55** (1997) 9935.
[97dH] den Hartog, S.G., van Wees, B.J., Nazarov, Yu.V., Klapwijk, T.M., Borghs, G.: Phys. Rev. Lett. **79** (1997) 3250.
[97K1] Katine, J.A., Eriksson, M.A., Adourian, A.S., Westervelt, R.M., Edwards, J.D., Lupu-Sax, A., Heller, E.J., Campman, K.L., Gossard, A.C.: Phys. Rev. Lett. **79** (1997) 4806.
[98H] Hauke, M., Jakumeit, J., Krafft, B., Nimtz, G., Förster, A., Lüth, H.: J. Appl. Phys. **84** (1998) 2034.
[98K] Kane, B.E., Facer, G.R., Dzurak, A.S., Lumpkin, N.E., Clark, R.G., Pfeiffer, L.N., West, K.W.: Appl. Phys. Lett. **72** (1998) 3506.
[98L] Liu, R.C., Odom, B., Yamamoto, Y., Tarucha, S.: Nature **391** (1998) 263.
[98U] Ulreich, S., Zwerger, W.: Superlattices and Microstructures **23** (1998) 719.
[99H] Henny, M., Oberholzer, S., Strunk, C., Heinzel, T., Ensslin, K., Holland, M., Schönenberger, C.: Science **284** (1999) 296.
[99T] Thywissen, J.H., Westervelt, R.M., Prentiss, M.: Phys. Rev. Lett. **83** (1999) 3762.